IEEE Access
Multidisciplinary | Rapid Review | Open Access Journal

Date of publication xxxx 00, 0000, date of current version xxxx 00, 0000.

Digital Object Identifier 10.1109/ACCESS.2017.DOI

A VLC Channel Model for Underground Mining Environments with Scattering and Shadowing

PABLO PALACIOS JÁTIVA[1], (Student Member, IEEE), CESAR A. AZURDIA-MEZA[1],(Member, IEEE), IVÁN SÁNCHEZ[2], FABIAN SEGUEL[3], DAVID ZABALA-BLANCO[4], ALI DEHGHAN FIROOZABADI[5], CARLOS A. GUTIÉRREZ[6], (Senior Member, IEEE), AND ISMAEL SOTO[3], (Member, IEEE)

[1]Department of Electrical Engineering, Universidad de Chile, Santiago 8370451, Chile
[2]Department of Telecommunications Engineering, Universidad de las Américas, Quito 170503, Ecuador
[3]Department of Electrical Engineering, Universidad de Santiago de Chile, Santiago 9170124, Chile
[4]Department of Computing and Industries, Universidad Católica del Maule, Talca 3466706, Chile
[5]Department of Electricity, Universidad Tecnológica Metropolitana, Santiago 7800002, Chile
[6]Faculty of Science, Universidad Autónoma de San Luis Potosí, San Luis Potosí 78290, México

Corresponding authors: Cesar A. Azurdia-Meza (e-mail: cazurdia@ing.uchile.cl) and Iván Sánchez (e-mail: ivan.sanchez.salazar@udla.edu.ec).

This work was supported in part by the Doctoral Fellowship Grant from ANID PFCHA/Doctorado Nacional/2019-21190489, in part by UDLA Telecommunications Engineering Degree, in part by Project STIC-AMSUD 19-STIC-08, in part by ANID FONDECYT Regular No. 1201893, in part by Vicerrectoría de Investigación y Desarrollo (VID) de la Universidad de Chile Proyecto ENL 01/20, in part by SENESCYT "Convocatoria abierta 2014-primera fase, Acta CIBAE-023-2014", in part by ANID FONDECYT Postdoctorado No. 3190147, and by Grupo de Investigación en Inteligencia Artificial y Tecnologías de la Información (IA&TI).

ABSTRACT Underground mining is an industry that preserves the miners' safety and efficiency in their work using wireless communication systems as a tool. In addition to communication links characterized by radio frequency signals, optical links in the visible light spectrum are under intense research for underground mining applications due to their high transmission rates and immunity to electromagnetic interference. However, the design of a robust visible-light communication (VLC) system for underground mining is a challenging task due to the harsh propagation conditions encountered in mining tunnels. To assist researchers in the design of such VLC systems, we present in this paper a novel channel model that incorporates important factors that influence the quality of the VLC link in underground mines. Features such as an arbitrary positioning and orientation of the optical transmitter and receiver, tunnels with irregular walls, shadowing by large machinery, and scattering by dust clouds are considered. These factors are integrated into a single modeling framework that lends itself for the derivation of compact mathematical expressions for the overall DC gain, the impulse response, the root mean square delay spread, and the received power of the proposed VLC channel model. Our analytical results are validated by computer simulations. These results show that the rotation and tilt of the transmitter and receiver, as well as the tunnels' irregular walls have a notorious influence on the magnitude and temporal dispersion of the VLC channel's line of sight (LoS) and non-LoS components. Furthermore, results show that shadowing reduces the LoS component's magnitude significantly. Our findings also show that scattering by dust particles contributes slightly to the total VLC channel gain, although it generates a large temporal dispersion of the received optical signal.

INDEX TERMS Channel impulse response, channel modeling, scattering, shadowing, underground mining, visible light communication.

I. INTRODUCTION

THE inherent working environment of underground mines is considered as very dangerous and unsafe due to inherent characteristics of the tunnels [1], as well as numerous external agents generated by regular mine operation such as dust, toxic components, sewage water, among others [2].

This article has been accepted for publication in a future issue of this journal, but has not been fully edited. Content may change prior to final publication. Citation information: DOI 10.1109/ACCESS.2020.3030615, IEEE Access

These factors make the underground mining environment be considered one of the most harsh environments for work and for establishing reliable communication links [3]. To manage day-to-day communication, along with the emergencies that can occur in this environment (landslides, fires, or intoxication of workers), an stable communication system is required [4]. This system must be designed to support applications focused on reliably localize and monitor infrastructure, and provide real-time information of all personnel within the tunnel infrastructure [5]. However, the physical conditions of the underground mines present a challenge for developing reliable and effective communication systems.

The geometric characteristics of the underground mine environment (the shape of walls and roof), as well as the interference and electromagnetic noise produced by the machinery employed in mining contributes to the difficulty of the communication system design [6]. In other words, the previous factors cause problems in the communication systems frequently used in mines, which are normally based on radio frequency (RF). Among the main complications of RF-based underground mining communications systems are a poor bit error rate (BER), a high delay spread in the signal, and a limited data transmission rate [7]. One solution to these issues comes from the combination of RF technologies with the novel scheme termed as visible light communication (VLC), which also provides continuous lighting within the underground mining environment [8].

VLC systems have several benefits, such as the use of unlicensed spectrum ranging from 400 THz to 800 THz, system elements with reasonable prices, and immunity to the electromagnetic interference, for instance [9], [10]. These advantages make VLC a good candidate to get a secure, robust, and reliable communication in underground mining environments [11]. Unfortunately, in this physically complex environment, the channel modeling tends to be more challenging in comparison to the traditional indoor scenarios where a VLC link is generally adopted [12].

An underground mine is composed by irregular tunnels, which present features that do not appear in typical indoor environments [13]. Factors such as dust particles that cause scattering, heavy machinery that generates shadowing, and non-flat walls and ceilings, which require angular positioning of the light emitting diodes (LEDs) and photodiodes (PDs) to provide better illumination and light reception inside the tunnel respectively are challenging for the VLC design in mining environments. On the other hand, it is well known that by modeling the communication channel, the overall system performance may be enhanced by using dedicated time/frequency techniques [14]. To the best of our knowledge, specifically applied to underground mining VLC systems, no channel model that considers its complicating characteristics has been presented. Based on an extensive review of the state of art (see Section II), and in an effort to design better underground mining communication systems, we present a VLC channel model that considers physical features that will have an effect in mining tunnels. We characterize and include in the underground mining VLC channel model the tilt and rotation of LEDs and PDs that impact the line of sight (LoS) and non-LoS components of the optical link. The characterization of non-flat walls in tunnels and their reflection effects in the optical signal are further considered. Finally, a scattering model that considers a disk-shaped distribution of the dust particles around the optical receiver, and a shadowing model that takes into account the entry of objects into the mining scenario are considered. The inclusion of the aforementioned parameters help us to understand the differences between a referential (typical indoor) VLC channel and the underground mining VLC channel. For channel modeling, we use the ray tracing methodology, which allows an accurate description of the interaction of rays emitted from LEDs to PDs within the underground mining environment.

The main contributions of this paper are summarized as follows:

1) Discussing the differences between the proposed underground mining VLC channel and the typical indoor VLC channel, which is used as a reference VLC channel model.
2) Adjusting and analyzing the effect of non-flat and non-regular tunnel walls, that generate non-orthogonal reflections, to properly model the optical signal in the proposed underground mining VLC channel.
3) Proposing a ray tracing-based underground mining VLC channel model that includes the effects of scattering and shadowing phenomena due to the presence of dust particles and objects (machinery), respectively. Firstly, the entry of objects that cause shadowing in the mining scenario is statistically modeled through a Poisson process. Secondly, the distribution and interaction of the dust particles are statistically modeled through a disk-shaped distribution, and by using the theories of Mie and Rayleigh scattering.

The remainder of this manuscript is organized as follows. In Section II, we provide an overview of the work related to existing VLC channel models applied to underground mines and their main characteristics. The traditional VLC channel model normally used in the literature is considered as a referential VLC channel model and explained in Section III. In Section IV, the effects of the positions of the LEDs and PDs, as well as the effect of the non-regular walls of the tunnels are derived and included in the proposed underground mining VLC channel model. Whereas in Sections V and VI, shadowing and scattering models are derived and included in the underground mining VLC channel model, respectively. In Section VII, we describe the mining scenario where we evaluate the proposed VLC channel model, present our results, and discuss our findings. Finally, conclusions of our work are described in Section VIII.

II. RELATED WORK

A. VLC APPLICATIONS IN UNDERGROUND MINES

In the state of the art, several applications for VLC systems in underground mines have been proposed [11], [15]–[20].

Among the most popular applications are those of location inside underground mining tunnels.

In [15], a hybrid system based on VLC and power line communication (PLC) for mines is proposed by showing its design and corresponding experimental demonstration. The channel model used for the evaluation of the VLC system is the Lambertian optical model, where only the LoS component is considered. Numerical results are presented in terms of the horizontal illumination and power received. These results indicate that the proposed VLC system can provide adequate lighting and good data transmission performance for mine communication applications. In [11], a solution to mitigate inter-cell interference (ICI) in an underground mining VLC system based on angle diversity receiver (ADR) is proposed. The implemented optical channel is based on the Lambertian model by considering the LoS and non-LoS components, as well as shot and thermal noises. The employed metrics to evaluate the solution are illuminance, root mean square (RMS) delay spread, user data rate (UDR), BER, and signal-to-interference-plus noise-ratio (SINR). The analysis of these metrics corroborates and validates the ICI mitigation in the VLC system applied to the underground mining environment. In [16], a method of positioning in underground mines based on the VLC technology is studied in detail. In this work, the author briefly provides theoretical concepts about the factors that could affect the mining VLC channel and how they would be involved in improving the capacity of the location system. In [17], [18], a VLC based system along with a trilateration technique for locating objects and people in an underground mining tunnel is proposed. In addition, the typical indoor VLC channel model is used to verify the performance of the proposed system. Localization error results show that the proposed application has better performance compared to typical localization technologies. In [19], another system based on a VLC scheme for localization by using three-dimensional trilateration is proposed. The channel model used for this work is the typical indoor VLC channel model. Location error, despite not having implemented its own VLC channel model for tunnels, is low compared to other RF-based technologies. In [20], a hybrid VLC-RF scheme by showing the implementation of a portable phasor measurement unit (PMU) for deep underground tunnels is proposed. Here, for the information download link, the proposed system uses the VLC technology. However, the authors highlight that a generic channel model for VLC systems in underground mining has not been proposed. Therefore, a typical indoor VLC channel model is employed. Experimental tests demonstrate the feasibility of the prototype, which has better performance compared to commercial PMUs.

The extreme conditions present throughout the tunnel are important characteristics to consider when we design VLC-based applications for underground mines. High levels of humidity, dust in the air, extreme heat, and machinery within the mine can affect the performance of the VLC system and applications based on it. Therefore, we believe that the revised VLC-based underground mining applications could improve their performance if they use our proposed VLC channel model in their development. In this context, our channel model proposal considers the most critical factors present in underground mines that are not considered in the traditional indoor VLC channel, which are positioning of LEDs and PDs, non-flat walls, shadowing, and scattering. Hence, VLC-based applications such as positioning, location, and real-time data transmission in underground mines would be more accurate and robust.

B. WORKS RELATED TO UNDERGROUND MINING VLC CHANNEL MODELS

In this subsection we present the most relevant and recent works reported in the literature that describe VLC channel models applied to underground mining environments [13], [21]–[25].

In [21], [22], a path loss model for a VLC channel applied to mines and two mining VLC communication scenarios, named mining roadway and mining working face, are proposed. In both works, the channel model is based on the well-known Lambertian optical model for indoor environments, where the LoS and non-LoS components are considered. The system performance is evaluated in terms of the path loss distribution and RMS delay spread in the first work [21]. Whereas in [22], the analysis focused on the channel impulse response (CIR) and received power. Both manuscripts demonstrate that the path loss exhibits a linear behavior in the log-domain. However, their results are based on a channel model that does not include in its analytical expression the main components that affect underground mining tunnels. In [23], an optical channel taking into account the reflections that occur in a confined structure, such as tunnels, is characterized. The adopted model is the Lambertian VLC channel model with the direct and diffuse components. The VLC system performance is evaluated through simulations, and the results are presented in terms of symbol error rate (SER). The results show that the VLC system robustness during tunnel construction, in terms of SER, is improved. Despite the fact that its results are obtained by simulating a tunnel scenario, the channel model limits them because it does not consider factors such as shadowing or scattering. In [24], the first analysis of a VLC channel model that considers an intrinsic characteristic of mines, such as dust particles, is presented. This paper studies the effects of coal dust particles in terms of the optical signal degradation. This phenomenon is analyzed using a Lambertian VLC channel model by considering LoS and non-LoS components, and the results are presented in terms of the CIR. These results show the optimized location of the optical transmitter to decrease the effect of dust on the degradation of the optical signal. However, the limitation of this work is not to include the effect of scattering directly in the theoretical model of the channel, since the analysis of its effect is developed as a factor external to the channel. In [13], the analysis on a VLC channel applied to underground mines is presented. The effect of shadowing and scattering are analyzed as channel-independent phenomena. Consequently, the effects of these phenomena are not included in the an-

alytical model of the VLC channel, so this omission would be its main limitation. The channel model is based again on the Lambertian optical scheme with LoS and non-LoS components. Therefore, angular variations of transmitter and receiver, and the effect of non-flat walls are not considered neither. The channel is evaluated in terms of the path loss and RMS delay spread. The results demonstrate the linear behavior of the path loss and depict differences in the RMS delay spread for different mining scenarios.

Finally, in [25], a neural network based approach is applied to derive an underground mine VLC channel model. The proposed channel model is based on nonlinear autoregressive exogenous parameters (NARX). Furthermore, the authors assumed a dynamic non-linear behavior of the optical channel. This work is experimentally validated in a dark gallery with a curved roof that emulates a mining tunnel. The main contribution of this work is the estimation of the parameters used for the neural network based VLC channel model applied to underground mining environments. However, a disadvantage of this work is that the model does not consider the scattering or shadowing phenomena in the estimated coefficients.

In summary, this literature review depicts that the channel model assumed by several authors for underground mining VLC environments is the same as the one used for indoor VLC environments. However, little or no evidence is presented to justify the assumed models and because they do not include the main factors of underground mines in their analytical expressions. In contrast to this works, we consider that in practical underground mining scenarios, LEDs would not always be located on the ceiling pointing directly downwards, the PDs would not be fixed pointing directly upwards since they could be installed in the helmets of the miners, and the shadowing and scattering phenomena must be included directly in the underground mining VLC channel model. These assumptions should be considered because they directly influence the quality of the received optical signal, which could affect the performance of the VLC system at the underground mine.

Moreover, in works that consider the optical signal reflections, reflective surfaces (roof or walls) are flat and regular. This idea would also be unpractical because of the tunnels are U-shaped and the walls are irregular and non-flat. On the contrary, we consider the irregularity of reflective surfaces by randomly modeling their normal vectors through their angles of rotation and tilt. These considerations influence the reflections that are modeled as random Lambertian point sources, and the radiation intensity of these "sources" is included in the underground mining VLC channel model.

C. SCATTERING AND SHADOWING MODELS APPLIED TO VLC INDOOR NON-MINING CHANNELS

The scattering and shadowing effects on the underground mining VLC channel has not been studied in depth in the literature, nevertheless, these effects have been analyzed in VLC channels applied to typical indoor environments [26]–[36].

One of the first investigations that considers shadowing in an indoor VLC environment is presented in [26]. In this work, the shadowing effect is produced by humans, who are modeled as cylinders. In [27], shadowing on the VLC indoor scenario is also generated by the human body where it is modeled as a cubic object. In [28], the authors continue with the trend of considering humans as blocking agents of the optical signal and modeling it as cylindrical objects. The novelty in previous work is to model the effect of shadowing on the VLC indoor stage as a Gaussian bi-modal distribution. In [29], a new study that considers shadowing in a light fidelity (LiFi)/RF hybrid indoor environment is proposed. The authors present the objects that cause shadowing as cylinders by affecting the LoS and non-LoS components. Finally, in [30], the authors considers the behavior and dimensions of the objects that produce shadowing as similar as possible to what happens in an underground mining scenario. In addition, a joint probability distribution to characterize the size and the position of the obstructions is introduced. According to our analysis of the literature, this work widely considers the real characteristics of a scenario in its statistical model. Therefore, we adapted its methodology for shadowing modeling that we developed in our underground mining VLC channel model proposal (see Section V). This adaptation is achieved by adjusting the obstacle entry model to the proposed mining scenario, by considering realistic obstacle dimensions and by establishing optical link blocking conditions typical of the tunnel.

On the other hand, the works related to scattering models applied to general RF communication schemes and optical systems are presented in [31]–[36]. In [31] and [32], a uniform distribution model of scatters is presented, which are located in a disc plane centered on the receiver. For this work, the receiver comes to be a mobile station. Although the focus of this work is not optical systems, the proposed model could be generalized for any type of technology, since it only presents the distribution of the particles that generate scattering. In [33] and [34], the study of optical wireless scattering modeling is presented as a non-LoS component over broad spectra. The modeling approach of these works is based on the concept that air molecules and suspended aerosols help to build optical scattering communication of non-LoS links by using near-infrared carriers to visible light and ultraviolet frequency bands. References [35] and [36] are the first works that consider the phenomenon of scattering in typical indoor VLC environments are presented. The authors locate possible scatters around a ring or an ellipse, depending on the number of lightning strikes on the scatterers. The total VLC channel is represented as the arithmetic sum of the LoS channel component and the channel components from the interaction between the optical transmitter, scatterer, and optical receiver.

Although there are several studies on the effect of scattering and shadowing in typical VLC indoors environments, in the authors' opinion, these phenomena have not been widely and properly analyzed in underground mining environments. In this context, only a few VLC channel modeling

manuscripts for underground mines consider blocking and dust particles. However, these proposals are not very realistic because they are based on the assumption of the typical indoor VLC channel. These works realistically model the tunnel features nor give a random approach to the physical phenomena present in underground mining scenarios. Furthermore, the reviewed works are limited since they do not analyze the effects that physical phenomena may have on the optical channel by not including them in the mathematical expression of the underground mining VLC channel model.

Then, in contrast to the studies reported in the literature, we included in the mathematical expressions of the LoS and non-LoS components of the proposed underground mining VLC channel model a weighting function to adequately describe the shadowing effect. This function is based on a Poisson process [30], which randomly describes the entry of objects in the underground mining VLC environment. Furthermore, to model the scattering effect, we considered the following premises: (1) The dust particles are uniformly distributed over a disc region centered on the installed PD in the helmet of the mining worker. (2) We consider the interaction of the optical link with the dust particles by modeling it through Mie scattering and Rayleigh scattering theories. Consequently, we derive and present a channel component produced by scattering of the optical signal, and its mathematical expression is included in the proposed mathematical model of the VLC channel for underground mines.

Finally, we have made a comparison between the characteristics considered by the main works on VLC channel modeling in underground mines found in the literature and our proposal. This comparison is summarized in Table 1. It can be seen that our proposal contemplates the main factors that exist in underground mines and that need to be considered in the channel model.

TABLE 1. Comparison between the proposed and state-of-art models.

Model	Characteristics			
	Tilt/Rotation LED/PD	Non-flat walls	Shadowing	Scattering
Riurean et. al. 2020 [25]	✗	✗	✗	✓
Morales et. al. 2019 [23]	✓	✗	✗	✗
Wang et. al. 2018 [13]	✗	✗	✓	✓
Wang et. al. 2017 [21]	✗	✗	✗	✗
Wang et. al. 2017 [22]	✗	✗	✗	✗
Zhai et. al. 2015 [24]	✗	✗	✗	✓
Our proposal	✓	✓	✓	✓

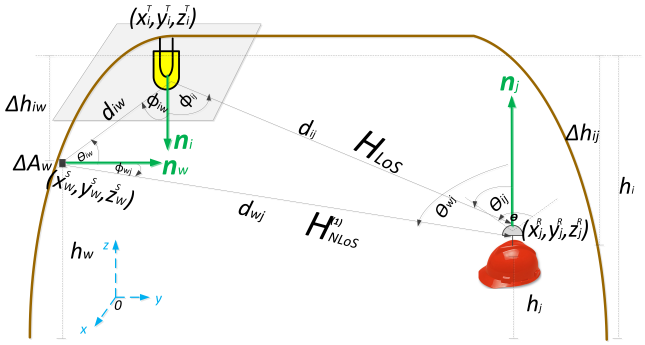

FIGURE 1. Downlink geometry of the light propagation for the reference underground mining scenario.

III. REFERENCE VLC CHANNEL MODEL APPLIED TO UNDERGROUND MINING

Usually, a closed indoor environment with reflective objects (walls and roof) for optical wireless downlink transmission is considered to model the standard indoor VLC channel. For our case, the geometric configuration of the downlink transmission applied to an ideal (referential) underground mining scenario is illustrated in Figure 1, where all its variables and constants will be described below. The VLC channel is the space between the LED and the PD and to model it, three different components must be analyzed: LEDs (light sources), PDs (light detectors), and the light propagation model.

A. LIGHT SOURCES

It is assumed that a LED is a point source that follows the Lambertian radiation pattern. Furthermore, the LED is assumed to operate within the linear dynamic range of the current-power characteristic curve and that it is fixed and oriented vertically downwards; its position is given by (x_i^T, y_i^T, z_i^T) in the Cartesian coordinate system. For the remainder of the manuscript, we consider the LED as an optical transmitter T_i, which belongs to a set of optical transmitters, where $i = 1, 2, ..., I$ and I is the total number of optical transmitters. Finally, we assume that each T_i has the same generalized Lambertian radiation pattern; therefore, the radiation intensity pattern $Ri(\phi_{ij})$ can be modeled as follows [9]:

$$Ri(\phi_{ij}) = \begin{cases} \frac{m+1}{2\pi}\cos^m(\phi_{ij}) & \text{if } -\pi/2 \leq \phi_{ij} \leq \pi/2 \\ 0 & \text{otherwise} \end{cases}, \quad (1)$$

where ϕ_{ij} is the radiance angle with respect to the normal vector to the T_i surface, which is $\boldsymbol{n}_i = [0, 0, -1]$, and $m = -1/log_2\left[cos(\Phi_{i1/2})\right]$ represents the Lambertian mode number of the T_i, which is a function of semi-angle at half power ($\Phi_{i1/2}$) of the T_i [9]. The subscript j of ϕ_{ij} will be defined in Section III-B.

B. LIGHT DETECTORS

We assume PDs as light detectors in the reception side of the VLC link. A PD is composed of a non-imaging concentrator (lens) and a physical active area A_p. In addition, for an ideal scenario, the PD may be assumed as fixed and vertically oriented upwards, where its position is represented by (x_j^R, y_j^R, z_j^R) in the Cartesian coordinate system. Hence, we consider the PD as an optical receiver R_j, which belongs to a set of optical receivers where $j = 1, 2, ..., J$ and J is

This article has been accepted for publication in a future issue of this journal, but has not been fully edited. Content may change prior to final publication. Citation information: DOI 10.1109/ACCESS.2020.3030615, IEEE Access

the total number of optical receivers. R_j collects the incident power produced by the light intensity of T_i. The effective collection area of the R_j detector acquires the form of [9]

$$A_{eff}(\theta_{ij}) = \begin{cases} A_p cos(\theta_{ij}) & \text{if } -\Theta/2 \leq \theta_{ij} \leq \Theta/2 \\ 0 & \text{otherwise} \end{cases}, \quad (2)$$

where θ_{ij} is the incidence angle with respect to the normal vector to the R_j surface, which is $\boldsymbol{n}_j = [0, 0, 1]$, and Θ is the PD field of view (FoV). The optical concentrator gain can be written as $g(\theta_{ij}) = \eta^2/sin^2(\Theta)$, being η the internal refractive index of the concentrator [9].

C. VISIBLE LIGHT PROPAGATION MODEL

In Sections III-A and III-B, the mathematical models of the LEDs and PDs were introduced. Here, we use them to derive the reference VLC channel model. In general, the VLC channel is modeled based on two optical components: the LoS component and non-LoS component. The LoS component directly results from the LED lighting falling on the PD. Therefore, the LoS link depends on LEDs and PDs parameters as seen above. The direct current (DC) gain of the LoS optical wireless channel is formulated by merging (1) and (2) by the following form [9]:

$$H_{LoS}(0; T_i, R_j) = \frac{(m+1)A_p}{2\pi d_{ij}^2} \cos^m(\phi_{ij}) \cos(\theta_{ij}) G(\theta_{ij}) \times rect\left(\frac{\theta_{ij}}{\Theta}\right), \quad (3)$$

where $rect\left(\frac{\theta_{ij}}{\Theta}\right) = 1$ for $0 \leq \theta_{ij} \leq \Theta$ and 0 otherwise; the Euclidean distance between T_i and R_j is denoted by d_{ij}, and $G(\theta_{ij})$=$T_s(\theta_{ij})$ $g(\theta_{ij})$ represents the combined gain of the optical filter and optical concentrator, respectively [9].

On the other hand, as a result of obstacles, indoor wall and ceiling surfaces, a diffuse component of the transmitted light is reflected by these elements. The sum of these reflections generates the non-LoS component of the VLC channel, termed as H_{NLoS}. A common model for diffuse reflection is the Lambertian reflectance where light is reflected with equal radiance in all directions. This model is based on the paradigm that the component $\|\mathrm{H}_{NLoS}^{(k)}\| \to 0$ when $k \to \infty$, where $H_{NLoS}^{(k)}$ is the non-LoS component after k bounces, and k is the total number of bounces [9], [16]. This concept implies two generalities: (1) Reflections caused by large number of bounces of k^{th} order would be negligible. (2) The first bounce comes to be the most important component that affects the received power and its temporal dispersion. Therefore, the H_{NLoS} component could be estimated by considering the first bounce, which is known as $H_{NLoS}^{(1)}$.

The DC gain of the non-LoS optical wireless channel can be calculated by adding all the components arriving at the R_j after being reflected in a surface, namely [9]

$$H_{NLoS}^{(1)}(0; T_i, R_j) = \frac{(m+1)A_p}{2\pi} \sum_{w=1}^{W} \frac{\Delta A_w \rho_w}{d_{iw}^2 d_{wj}^2} \cos^m(\phi_{iw}) \times cos(\theta_{iw}) cos(\phi_{wj}) \cos(\theta_{wj}) G(\theta_{wj}) \times rect\left(\frac{\theta_{wj}}{\Theta}\right), \quad (4)$$

where ΔA_w denotes the w^{th} area of the considered reflective element w, whose reflection coefficient and position are respectively represented by ρ_w and (x_w^S, y_w^S, z_w^S). W is the total number of reflective elements considered in the scenario. The incidence angle with respect to the normal vector to the reflective element w ($\boldsymbol{n}_w = [0, 1, 0]$) and the radiance angle of the light component reaching the reflective element w are symbolized with θ_{iw} and ϕ_{iw}, respectively. The angles of incidence and radiance denoted by θ_{wj} and ϕ_{wj} respectively are measured with respect to the light component that is reflected in the reflective element w and reaches R_j. Finally, the Euclidean distances between T_i and the reflective element w, and between the reflective element w and R_j are given by d_{iw} and d_{wj}, respectively.

As we mentioned, the analysis of VLC system components that we present in this section focuses on a reference VLC channel model. Therefore, despite applying it to a tunnel, we do not consider intrinsic factors and features of the underground mine. However, this observation gives us a overall framework and naturally leads us to Sections IV, V and VI, where we discuss more details about the development of the proposed underground mining VLC channel model. In Section IV we analyze and consider in the underground mining VLC channel model to be proposed, the position characteristics (rotation and tilt) of the system elements (LEDs and PDs), and the effect of the non-regular and non-flat walls of the tunnels. Then, in Section V, we statistically characterize the shadowing and add it to the VLC underground mining channel components derived in Section IV. The scattering distribution in the underground mining scenario, its statistical characterization, and its channel component are derived in Section VI. At the end of this section, the closed mathematical expression of the proposed underground mining VLC channel model is presented.

IV. POSITION CHARACTERIZATION OF LEDS AND PDS, AND NON-FLAT WALLS MODELING

A. TILTED AND ROTATED LEDS AND PDS

In a real underground mining scenario, LED luminaries are normally installed on the ceiling or on the walls of the tunnels. To facilitate maintenance and replacement work, the placement of LEDs in the curved sections between the wall and the ceiling of the tunnel is preferred. When we place the T_i on the tunnel walls, it normally does not point vertically downwards. A convenient way to describe the orientation of the T_i is to use two separate angles that show the tilt and rotation on the axes of the reference coordinate system. The tilt angle with respect to the z-axis is represented by β_i, which takes values in range of $[90°, 180°)$ and the rotation angle

This article has been accepted for publication in a future issue of this journal, but has not been fully edited. Content may change prior to final publication. Citation information: DOI 10.1109/ACCESS.2020.3030615, IEEE Access

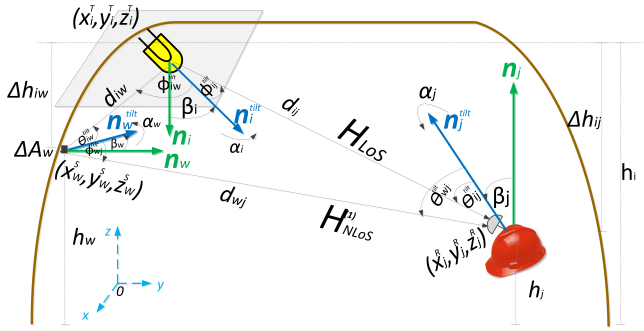

FIGURE 2. Downlink light propagation geometry for the proposed underground mining scenario.

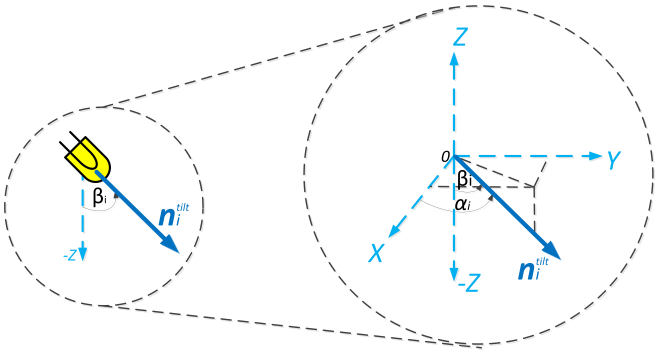

FIGURE 3. Transmitter position characteristics.

with respect to the x-axis is denoted as α_i, which is defined in the interval $[0°, 360°)$. Both ranges of values are based on the characteristics of the underground mining scenario and work related to LED positioning [37]–[39]. These elementary angles are represented in Figures 2 and 3.

It is evident that the orientation of the T_i determines its normal vector $\boldsymbol{n}_i$. Therefore, $\boldsymbol{n}_i$ after the tilt and rotation of the T_i is termed by $\boldsymbol{n}_i^{tilt}$. This orientation also affects ϕ_{ij}, which is now denoted as ϕ_{ij}^{tilt}. The effect of these considerations is directly distinguished in the term $\cos(\phi_{ij}^{tilt})$ of the LoS channel component, which is based on the vector concepts as follows:

$$\cos(\phi_{ij}^{tilt}) = \frac{V_{i-j} \cdot \boldsymbol{n}_i^{tilt}}{\|V_{i-j}\| \|\boldsymbol{n}_i^{tilt}\|}, \tag{5}$$

where the vector from T_i to R_j is denoted by V_{i-j}, the notation $\|\cdot\|$ denotes the 2-norm, and $\cdot$ represents the product dot operation. Also, for vector concepts, $\|V_{i-j}\|= d_{ij}$, $\|\boldsymbol{n}_i^{tilt}\|$=1, and $\boldsymbol{n}_i^{tilt}$ can be represented in terms of α_i and β_i as $\boldsymbol{n}_i^{tilt} = [\sin(\beta_i)\cos(\alpha_i), \sin(\beta_i)\sin(\alpha_i), -\cos(\beta_i)]$. T_i positioning characteristics are shown in Figure 3. Notice that the z-component of the $\boldsymbol{n}_i^{tilt}$ is negative since the T_i is pointing downwards. Furthermore, $V_{i-j} = [x_j^R - x_i^T, y_j^R - y_i^T, -\Delta h_{ij}]$, assuming that Δh_{ij} is the difference height between T_i and R_j, that is z_i^T-$z_j^R = \Delta h_{ij}$. Consequently, the expression (5) can be rewritten in the following form:

$$\cos(\phi_{ij}^{tilt}) = \frac{[x_j^R - x_i^T, y_j^R - y_i^T, -\Delta h_{ij}]}{d_{ij}} \cdot [\sin(\beta_i)\cos(\alpha_i), \sin(\beta_i)\sin(\alpha_i), -\cos(\beta_i)]. \tag{6}$$

On the other hand, when we install R_j in the helmets of the mining workers, R_j does not always point vertically upward due to the nature of the person's head movement. As in T_i, the orientation of R_j can be described by using the angles of tilt and rotation on the reference coordinate system. Here, the tilt angle with respect to the z-axis is denoted as β_j, which takes values in range of $[0°, 90°)$, and the rotation angle with respect to the x-axis is denoted with α_j that can be values in range of $[0°, 180°)$. Both range of values are based on the characteristics of the underground mining scenario, the range of motion of a person's head, and works related to PD positioning [40]–[42]. These angles are displayed in Figures 2 and 4 for clarification purposes.

The previous considerations for the orientation of R_j change its $\boldsymbol{n}_j$ and θ_{ij}, which are now denoted as $\boldsymbol{n}_j^{tilt}$ and θ_{ij}^{tilt}, respectively. Furthermore, this effect is directly noticeable in the term $\cos(\theta_{ij}^{tilt})$ of the LoS channel component, which is based on the vector concepts as follows:

$$\cos(\theta_{ij}^{tilt}) = \frac{V_{j-i} \cdot \boldsymbol{n}_j^{tilt}}{\|V_{j-i}\| \|\boldsymbol{n}_j^{tilt}\|}, \tag{7}$$

where V_{j-i} is the vector from R_j to T_i. For vector concepts, we also consider that $\|V_{j-i}\|= d_{ij}$, $\|\boldsymbol{n}_j^{tilt}\|$=1, $\boldsymbol{n}_j^{tilt} = [\sin(\beta_j)\cos(\alpha_j), \sin(\beta_j)\sin(\alpha_j), \cos(\beta_j)]$, and $V_{j-i} = [x_i^T - x_j^R, y_i^T - y_j^R, \Delta h_{ij}]$ as can be seen in Figure 4. Consequently, the expression (7) can be rewritten as

$$\cos(\theta_{ij}^{tilt}) = \frac{[x_i^T - x_j^R, y_i^T - y_j^R, \Delta h_{ij}]}{d_{ij}} \cdot [\sin(\beta_j)\cos(\alpha_j), \sin(\beta_j)\sin(\alpha_j), \cos(\beta_j)]. \tag{8}$$

Finally, in order to include the effect of the orientation of T_i and R_j in the proposed underground mining VLC channel model, we replace the expressions (6) and (8) in the mathematical expression of the LoS channel component expressed in (3) to obtain a precise model for H_{LoS} that is given by (9).

B. NON-FLAT AND NON-REGULAR TUNNEL WALLS

Usually, in the modeling of reflective elements for traditional interior environments such as offices and hospitals, the walls are considered as ideal reflective elements. Among the ideal features assumed can be mentioned: perpendicularity with respect to the ceiling, regularity, and flat surface. However, these assumptions do not make sense in underground mines since most tunnels are U-shaped, irregular, and non-flat. Therefore, it is necessary to adequately model the effect of the tunnel walls to include them in the proposed underground mining VLC channel model and analyze their impact on system performance.

As mentioned in Section III-C, each reflective element is modeled with the Lambertian reflectance, so each of them

This article has been accepted for publication in a future issue of this journal, but has not been fully edited. Content may change prior to final publication. Citation information: DOI 10.1109/ACCESS.2020.3030615, IEEE Access

$$H_{LoS}(0;T_i,R_j) = \frac{(m+1)A_p}{2\pi d_{ij}^{m+3}} \left\{ \left[x_j^R - x_i^T, y_j^R - y_i^T, -\Delta h_{ij}\right] \cdot \left[\sin(\beta_i)\cos(\alpha_i), \sin(\beta_i)\sin(\alpha_i), -\cos(\beta_i)\right] \right\}^m$$
$$\times \left\{ \left[x_i^T - x_j^R, y_i^T - y_j^R, \Delta h_{ij}\right] \cdot \left[\sin(\beta_j)\cos(\alpha_j), \sin(\beta_j)\sin(\alpha_j), \cos(\beta_j)\right] \right\} G(\theta_{ij}^{tilt}) rect\left(\frac{\theta_{ij}^{tilt}}{\Theta}\right). \quad (9)$$

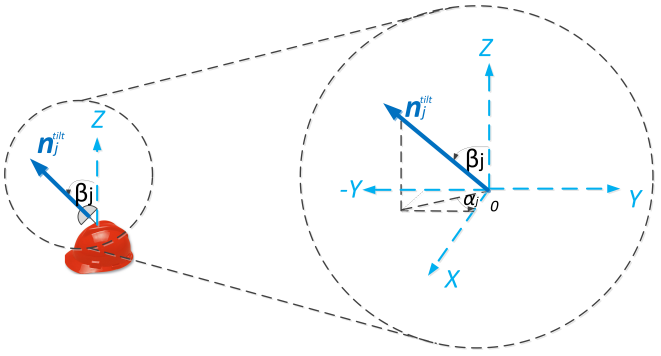

FIGURE 4. Receiver position characteristics.

can be considered as a Lambertian point source. However, in the underground mining context, the irregularity of the surface of each reflective element implies that the radiation intensity of this source and the direction of the reflected light are not deterministic. Additionally, in ideal reflective elements, their normal vectors are orthogonal to their surfaces and everyone pointing in the same direction. This situation does not occur in a underground mining scenario. Here, each reflective element has an irregular surface. Therefore, their normal vectors are not orthogonal to their surface, and they point in different directions.

As happened with the normal vectors described in Section IV-A, the normal vector $\boldsymbol{n}_w$ of each reflective element w can be described in terms of their tilt and rotation angles on the axes of the reference coordinate system. Here, the tilt angle with respect to the z-axis is denoted as β_w, which belongs to the range of $[0°, 180°)$ and the rotation angle with respect to the x-axis is denoted as α_w and takes values in range of $[0°, 180°)$. Both intervals are based on the characteristics and limitations that exist in a underground mining scenario (see Figure 2).

The introduced features for the orientation of each reflective element w changes its normal vector $\boldsymbol{n}_w$, and its angles θ_{iw} and ϕ_{wj}, which are now termed by $\boldsymbol{n}_w^{tilt}$, θ_{iw}^{tilt} and ϕ_{wj}^{tilt}, respectively. Additionally, the tilt and rotation of T_i and R_j affects this channel component in terms of the angles ϕ_{iw} and θ_{wj}, which are redefined by ϕ_{iw}^{tilt} and θ_{wj}^{tilt}, respectively. Therefore, the irregular walls of the tunnels along with the orientation of T_i and R_j directly affect the non-LoS component of the underground mining VLC channel.

The effect of these considerations is noticeable in terms of the following cosines: $\cos(\phi_{iw}^{tilt})$, $\cos(\theta_{iw}^{tilt})$, $\cos(\phi_{wj}^{tilt})$ and $\cos(\theta_{wj}^{tilt})$ in the following form:

$$\cos(\phi_{iw}^{tilt}) = \frac{V_{i-w} \cdot \boldsymbol{n}_i^{tilt}}{\|V_{i-w}\| \|\boldsymbol{n}_i^{tilt}\|}, \quad (10)$$

where V_{i-w} is the vector from T_i to w, $\|V_{i-w}\| = d_{iw}$, and $V_{i-w} = \left[x_w^S - x_i^T, y_w^S - y_i^T, -\Delta h_{iw}\right]$, assuming that Δh_{iw} is the difference height between T_i and w.

$$\cos(\theta_{iw}^{tilt}) = \frac{V_{w-i} \cdot \boldsymbol{n}_w^{tilt}}{\|V_{w-i}\| \|\boldsymbol{n}_w^{tilt}\|}, \quad (11)$$

where V_{w-i} is the vector from w to T_i, $\|V_{w-i}\| = d_{iw}$, $\|\boldsymbol{n}_w^{tilt}\|$=1, $\boldsymbol{n}_w^{tilt}$ can be represented in terms of α_w and β_w, that is $\boldsymbol{n}_w^{tilt} = [\sin(\beta_w)\cos(\alpha_w), \sin(\beta_w)\sin(\alpha_w), \cos(\beta_w)]$ and $V_{w-i} = \left[x_i^T - x_w^S, y_i^T - y_w^S, \Delta h_{iw}\right]$.

$$\cos(\phi_{wj}^{tilt}) = \frac{V_{w-j} \cdot \boldsymbol{n}_w^{tilt}}{\|V_{w-j}\| \|\boldsymbol{n}_w^{tilt}\|}, \quad (12)$$

where V_{w-j} is the vector from w to R_j, $\|V_{w-j}\|$=d_{wj}, and $V_{w-j} = \left[x_j^R - x_w^S, y_j^R - y_w^S, -\Delta h_{wj}\right]$, assuming that Δh_{wj} is the difference height between w and R_j.

$$\cos(\theta_{wj}^{tilt}) = \frac{V_{j-w} \cdot \boldsymbol{n}_j^{tilt}}{\|V_{j-w}\| \|\boldsymbol{n}_j^{tilt}\|}, \quad (13)$$

where V_{j-w} is the vector from R_j to w, $\|V_{j-w}\| = d_{wj}$, and $V_{j-w} = \left[x_w^S - x_j^R, y_w^S - y_j^R, \Delta h_{wj}\right]$.

All the previous definitions allow us to reform the expressions (10), (11), (12), and (13). Finally, in order to include the effect of non-regular walls of the tunnels in the proposed underground mining VLC channel model, we replace these new expressions in the mathematical model of the non-LoS channel component expressed in (4). As a consequence, we obtain an exact expression for $H_{NLoS}^{(1)}$ given by (14).

V. STATISTICAL SHADOWING MODEL CAUSED BY RANDOM OBSTRUCTIONS

A physical phenomenon that particularly conditions wireless communication links in underground mining environments is the shadowing due to its great dependence on having line of sight, by affecting the system performance. Because of the underground mining infrastructure, in which there are large machinery and vehicles that move by the tunnels, the effect of shadowing must be considered in order to derive a reasonable underground mining VLC channel model.

In our shadowing study, we are assuming that the PD is mounted on the miners' helmet. Therefore, due to the location of T_i, we do not consider the shadowing effect that could occur when miners (human obstacles) block the VLC link. Because of the real characteristics of the tunnels, we

$$H_{NLoS}^{(1)}(0;T_i,R_j) = \frac{(m+1)A_p}{2\pi}\sum_{w=1}^{W}\frac{\Delta A_w \rho_w}{d_{iw}^{m+3}d_{wj}^{4}}\left\{\left[x_w^S - x_i^T, y_w^S - y_i^T, -\Delta h_{iw}\right]\cdot[\sin(\beta_i)\cos(\alpha_i),\sin(\beta_i)\sin(\alpha_i),-\cos(\beta_i)]\right\}^m$$
$$\times\left\{\left[x_i^T - x_w^S, y_i^T - y_w^S, \Delta h_{iw}\right]\cdot[\sin(\beta_w)\cos(\alpha_w),\sin(\beta_w)\sin(\alpha_w),\cos(\beta_w)]\right\}$$
$$\times\left\{\left[x_j^R - x_w^S, y_j^R - y_w^S, -\Delta h_{wj}\right]\cdot[\sin(\beta_w)\cos(\alpha_w),\sin(\beta_w)\sin(\alpha_w),\cos(\beta_w)]\right\}$$
$$\times\left\{\left[x_w^S - x_j^R, y_w^S - y_j^R, \Delta h_{wj}\right]\cdot[\sin(\beta_j)\cos(\alpha_j),\sin(\beta_j)\sin(\alpha_j),\cos(\beta_j)]\right\}G(\theta_{wj}^{tilt})rect\left(\frac{\theta_{wj}^{tilt}}{\Theta}\right). \quad (14)$$

only consider the optical link blockage caused by vehicles and obstacles moving along the tunnels.

A. ASSUMPTIONS CONSIDERED TO MODEL SHADOWING STATISTICALLY

Shadowing comes from non-quantitative obstructions (vehicles and obstacles) that randomly enter to the underground mining area with particular characteristics (size, position, income intensity, etc.). In addition, we consider that numerous LEDs illuminate the work area in underground mines completely. Therefore, it is impossible for all optical links to be completely blocked. However, vehicles entering the underground mining area can block certain optical links and partially attenuate the transmitted signal strength.

According to the literature, shadowing applied to VLC systems has been modeled as a binomial Gaussian distribution [13] and as a Poisson process [30]. After a comparative analysis of models that fit the real characteristics of the shadowing phenomenon in underground mines, we follow and extrapolate to our analysis a statistical methodology for shadowing modeling [30]. This approach utilizes a Poisson process to describe the appearance of obstructions in the VLC environment, a probability density function to characterize the size and position of the obstructions, such as vehicles or heavy machinery, and a weighting function to describe the shadowing effect. The weighting function will be described in detail and derived in Section V-C.

B. DESCRIPTION OF THE UNDERGROUND MINING SCENARIO WITH OPTICAL LINK BLOCKING

We consider a VLC link obstruction/non-obstruction underground mining scenario as shown in Figure 5. In order to easily represent the underground mining environment and without losing the generality, we assume that the tunnel area to be analyzed is cubic with the following dimensions: length (X), width (Y), and height (Z). For a better description of the scenario, we consider a line segment AB, where the point A is the Cartesian coordinate where T_i is located and the point B is the Cartesian coordinate where R_j is located. We observe that the magnitude of line segment AB matches to the magnitude of d_{ij}.

For our model, we discard the thickness of the obstruction and consider the point V, whose coordinates are represented by $(x_v, y_v, 0)$, as the midpoint of the projection of the obstruction in the x-y plane. Furthermore, the line segment CD

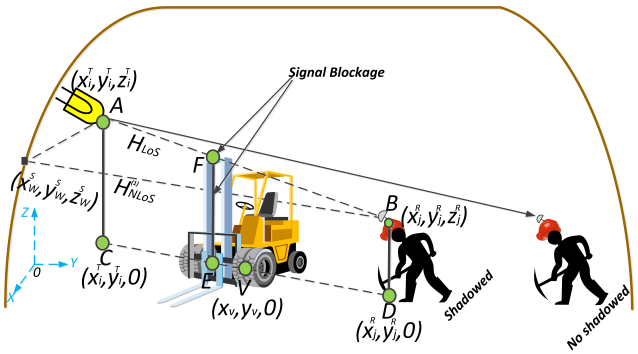

FIGURE 5. Schematic diagram of the AB optical link being blocked by a mobile obstruction with width w_v and height h_v.

represents the projection of line segment AB in the x-y plane, whose coordinates of the points C and D are $(x_i^T, y_i^T, 0)$, $(x_j^R, y_j^R, 0)$ respectively. Finally, we consider a perpendicular line segment to CD from the point $(x_v, y_v, 0)$ with the point E being the foot point and, thus, we construct a line EF parallel to the z-axis through point E, where the point F denotes the intersecting point with the segment AB.

C. PROPOSED STATISTICAL SHADOWING MODEL

Based on the work presented in [30], we statistically model the entry of obstructions into the underground mining environment and, consequently, the shadowing produced considering the following statistical assumptions: (1) We assume that there are not obstructions in the scenario at the beginning time. (2) For the no-shadowed case, VLC channel components are not affected. On the other hand, for the shadowed situation, a weighting function P_{ij} is introduced to describe the random shadowing. P_{ij} describes the probability that the LoS optical link is not blocked. (3) We assume the entry of obstructions to the underground mining area as a Poisson process N_t with an intensity parameter ϵ. Furthermore, each obstruction is independently and identically distributed with its own dimensions (width w_o and height h_o) and position $(x_o\ ,\ y_o)$. Therefore, the blocking or not of the optical link that the obstacles can cause are independent of each other. (4) We denote possible obstructions entering the scenario within a period of time t as (w_1, h_1, x_1, y_1), (w_2, h_2, x_2, y_2),...,$(w_{N_t}, h_{N_t}, x_{N_t}, y_{N_t})$. (5) We denote p_v as the probability that the LoS optical link (line segment AB) is blocked by (w_v, h_v, x_v, y_v) where v takes values from

This article has been accepted for publication in a future issue of this journal, but has not been fully edited. Content may change prior to final publication. Citation information: DOI 10.1109/ACCESS.2020.3030615, IEEE Access

1 to N_t and p_1, p_2,..., p_{N_t} are independent and identically distributed. Consequently, P_{ij} can be written as [30]

$$P_{ij} = \exp\left[-\epsilon E(p_v)t\right], \tag{15}$$

where $E(p_v)$ is the expected value of p_v. Now, we must find the specific physical and geometric conditions that mathematically demonstrate when the optical link is blocked by some obstruction (w_v, h_v, x_v, y_v). Based on the geometry of Figure 5, we can summarize two main conditions [30]: (1) Half of w_v must be greater than or equal to the distance from the point (x_v, y_v) to the segment CD, namely $w_v/2 \geq d(x_v, y_v)$. (2) h_v must be greater than or equal to the length of EF, namely $h_v \geq s(x_v, y_v)$.

Since the coordinates of the points A and B are known, we can formulate the expressions of $d(x_v, y_v)$ and $s(x_v, y_v)$ as follows:

$$d(x_v, y_v) = \frac{|(y_i^T - y_j^R)x_v - (x_i^T - x_j^R)y_v - x_j^R y_i^T + x_i^T y_j^R|}{\sqrt{(y_i^T - y_j^R)^2 + (x_i^T - x_j^R)^2}}, \tag{16}$$

$$s(x_v, y_v) = \frac{(y_i^T - y_j^R)^2 + (x_i^T - x_j^R)^2 + (x_v - x_j^R)^2}{2\sqrt{(y_i^T - y_j^R)^2 + (x_i^T - x_j^R)^2}} + \frac{(y_v - y_j^R)^2 - [(x_v - x_i^T)^2 + (y_v - y_i^T)^2]}{2\sqrt{(y_i^T - y_j^R)^2 + (x_i^T - x_j^R)^2}} + z_j^R. \tag{17}$$

As the entry of possible obstructions to the tunnel is not deterministic, we denote functions of joint probability density for w_v and h_v as $g_v(w, h)$ and for x_v and y_v as $f_v(x, y)$, respectively. It is worth noting that these joint probability density functions can be adapted and chosen depending on the actual situation of the scenario to be modeled, in our case, the underground mining scenario. Consequently, $E(p_v)$ and P_{ij} are presented in (18) and (19) [30].

Finally, we include the shadowing characterization and its effect in the LoS channel component expressed in (9) by including the weighted function P_{ij} in its mathematical expression. In addition, we also consider the shadowing effect in the non-LoS channel component expressed in (14) by including the weighted functions P_{iw} and P_{wj} in its mathematical expression. These weighted functions are obtained through the same statistical process to obtain P_{ij} and they represent possible blockages in the optical link between T_i and the reflective element w, and the optical link between w and R_j, respectively. Therefore, the new mathematical expressions obtained by multiplying the LoS an non-LoS channel components by their corresponding weighting function are denoted as $H_{LoS_{(sh)}}$ and $H^{(1)}_{NLoS_{(sh)}}$ respectively, and expressed as follows:

$$H_{LoS_{(sh)}}(0; T_i, R_j) = H_{LoS}(0; T_i, R_j)P_{ij}, \tag{20}$$

$$H^{(1)}_{NLoS_{(sh)}}(0; T_i, R_j) = H^{(1)}_{NLoS}(0; T_i, R_j)P_{iw}P_{wj}. \tag{21}$$

VI. STATISTICAL SCATTERING MODEL PRODUCED BY DUST PARTICLES

In general, the scattering produced by the suspended dust is generally despicable in traditional indoor environments, such as offices, hospitals, or non-dangerous industries. Therefore, in these scenarios, VLC systems are not generally affected by dust particles. Instead, in underground mines, large amounts of dust are originated by crushing, grinding, flying, and drilling the rock within the mine. Hence, it is necessary to model the scattering effect and introduce it into the underground mining VLC channel model. Consequently, we perform an in-depth analysis to derive the appropriate mathematical model that fits this physical phenomenon.

We propose an stochastic model that provides a simple physical interpretation, but in accordance with the real characteristics of the underground mining scenarios. The model that we introduce is based on the theory of absorption and dispersion of photons that travel through the atmosphere. Also, we model the distribution of the scatterers elements (dust particles) based on the unified disk scattering model (UDSM), which is revealed in [32]. This model allows us to control the distribution of the scatterers by using a factor, which controls the concentration pattern of the scatterers.

A. SCATTERERS DISTRIBUTION MODEL CONSIDERATIONS

The outline of the scatterers distribution, as well as the geometric considerations that we adopt in our analysis are displayed in Figure 6. By considering the underground mining environment, we assume that at the beginning, T_i is free of scatterers to their surroundings and the height where they are positioned is greater than the height where R_j is located. Furthermore, we assume that the scatterers are randomly and independently distributed within a disk-shaped area of radio R_r centered on R_j. These scatterers are called local scatterers.

We consider that within the disk centered on R_j, there are numerous local scatterers S_n, where $n = 1, 2, ..., N$. Theoretically, the number of scatters N could tend to infinite. The location of each local scatterer is represented by its polar coordinates as $(r_n, \theta_{S_n - j})$, where r_n is the distance from the n^{th} local scatterer to R_j and $\theta_{S_n - j}$ represents the angle between the distance vector from the n^{th} local scatterer to R_j and $\boldsymbol{n}_j^{tilt}$. Owing to the high path loss that occurs in VLC systems, we discarded the contribution of scatterers outside the assumed disk-shaped area (remote scatterers). Furthermore, we assume that the light beam from the optical link transmitted from T_i travels through the atmosphere, impacts some of the local scatterers, and reaches R_j after a single bounce.

After the optical signal hits the local scatterer, it can be absorbed or dispersed. Therefore, R_j could receive signals from diverse directions, which are only determined by the distribution of local scatterers. We define the Euclidean distance of the transmitted optical link between T_i and S_n as d_{i-S_n} and the radiance angle between the T_i and S_n as

This article has been accepted for publication in a future issue of this journal, but has not been fully edited. Content may change prior to final publication. Citation information: DOI 10.1109/ACCESS.2020.3030615, IEEE Access

$$E(p_v) = \int_0^X \int_0^Y \left[\int\int_{\{(w,h):w \geq 2d(x,y), h \geq s(x,y)\}} g_v(w,h) dw\, dh \right] f_v(x,y) dx\, dy, \tag{18}$$

$$P_{ij} = \exp\left\{ -\epsilon \left\{ \int_0^X \int_0^Y \left[\int\int_{\{(w,h):w \geq 2d(x,y), h \geq s(x,y)\}} g_v(w,h) dw\, dh \right] f_v(x,y) dx\, dy \right\} t \right\}. \tag{19}$$

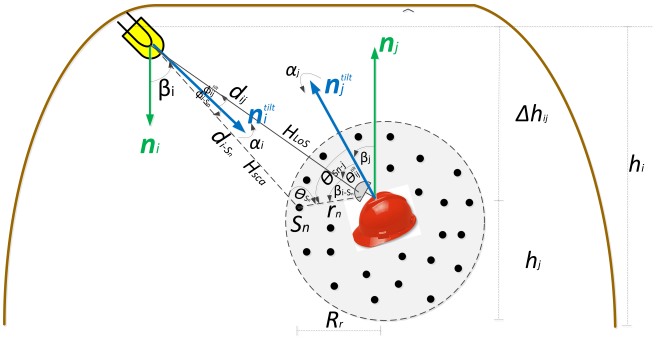

FIGURE 6. Outline of the geometric scattering pattern.

ϕ_{i-S_n}. Therefore, we can describe the probability distribution function (PDF) of the UDSM as follows [32]:

$$p_{r_n}(r_n, \theta_{S_n-j}) = \begin{cases} \frac{(a+1)(r_n)^a}{2\pi R_r^{(a+1)}}, & \text{if } -\pi \leq \theta_{S_n-j} \leq \pi \\ & \text{and } 0 < r_n \leq R_r \\ 0 & \text{otherwise} \end{cases}, \tag{22}$$

where $a \geq 0$ is the shape factor that corresponds to a real value. This value controls the distribution of the scatterers within the disk-shaped area (see Figure 6). The UDSM generally depends on r_n, except for $a = 0$ and θ_{S_n-j} is uniformly distributed in the interval $[-\pi, \pi]$. In other words, the UDSM obeys to a circularly symmetric scattering model. For an specific R_r, we can choose values of a between 0 and 1, which only includes scatterers near to R_j and is useful for modeling urban and suburban propagation areas. Due to the real characteristics of the underground mine and the work carried out inside it, we obtain a purely uniform distribution of the scatterers by fixing a to 1. Therefore, the expression (22) acquires the form of

$$p_{r_n}(r_n, \theta_{S_n-j}) = \begin{cases} \frac{r_n}{\pi R_r^2}, & \text{if } -\pi \leq \theta_{S_n-j} \leq \pi \\ & \text{and } 0 < r_n \leq R_r \\ 0 & \text{otherwise} \end{cases}. \tag{23}$$

Notice that if the value of a increases, the scatterers are concentrated in a hollow disk-shaped area centered on R_j.

B. ANALYSIS OF THE INTERACTION BETWEEN THE OPTICAL LINK AND LOCAL SCATTERERS

To characterize the effect of the interaction between the optical link and local scatterers, we assume a scenario where the light ray emitted by T_i travels through the atmosphere, interacts with S_n effective scatterers, and reaches R_j. To derive a generalized theoretical approach, we present a reference model based on the assumption that the number of local scatterers can tend to infinity, ($N \to \infty$). Consequently, the total diffuse channel components produced by the scattered signals can be represented as a superposition of an infinite number of plane waves coming from different directions determined by the distribution of the local scatterers. We assume that each scatterer S_n introduces a coefficient G_n. This gain is inversely proportional to N and directly proportional to the average of the dust particle reflection coefficient $\overline{\rho_s}$, that is, $G_n = \overline{\rho_s}/N$.

As the light beam (photons) after leaving T_i travels through the atmosphere, we can model the interaction of light with dust particles in the atmosphere as a combination of light absorption and scattering events [33], [34], whose coefficients of absorption and dispersion are represented by k_a and k_s, respectively. It is important to mention that when a photon is absorbed by some dust particle, it is annihilated and does not reach the R_j. Therefore the coefficient k_a is not considered in our analysis.

On the other hand, when a light link collides with a dust particle and it scatters, its path is altered before continuing to travel through the atmosphere, as can be see in Figure 6. Therefore, the coefficient k_s must be considered in the analysis. To describe this path change in a stochastic way, we consider the pair of angles $(\phi_{i-S_n}, \theta_{S_n})$, where ϕ_{i-S_n} is the radiance angle measured between $\boldsymbol{n}_i^{tilt}$ and the vector from T_i to S_n, and θ_{S_n} is the scattering angle. To validate these considerations, we must obtain the PDF of the phase function that describes the angular distribution of the scattered optical power.

This phase function can be modeled as a weighted combination of the generalized Rayleigh scattering phase function p_{ray} and the phase function based on the Mie scattering theory, represented by the generalized Henyey-Greenstein function p_{mie}. In particular, for $0 \leq \phi_{i-S_n} \leq \pi/2$ and $0 \leq \theta_{S_n} \leq \Theta$, these functions are expressed as [33], [34]

$$p_{ray}(\mu) = \frac{3[1 + 3\gamma + (1-\gamma)\mu^2]}{16\pi(1+2\gamma)}, \tag{24}$$

$$p_{mie}(\mu) = \frac{1-g^2}{4\pi} \left[\frac{1}{\sqrt{(1+g^2-2g\mu)^3}} + \frac{f(3\mu^2-1)}{2\sqrt{(1+g^2)^3}} \right], \tag{25}$$

where $\mu = cos(\theta_{S_n})$, and γ, g and f are atmospheric model parameters.

The contribution that the scattering generates is determined in terms of the type of dust particle according to its diameter. This contribution is governed by atmospheric

This article has been accepted for publication in a future issue of this journal, but has not been fully edited. Content may change prior to final publication. Citation information: DOI 10.1109/ACCESS.2020.3030615, IEEE Access

composition and modeled by the weighting parameters k_r and k_m, which are Rayleigh scattering and Mie scattering coefficients, respectively. In addition, we know that k_s=k_r+k_m [33], [34]. The interaction of these phase functions follows a Bernoulli distribution, i.e. the probability that the photon is modeled as p_{ray} is k_r/k_s and the probability that the photon is modeled as p_{mie} is k_m/k_s. Therefore, the overall phase function along with its respective PDF is given by [33], [34]

$$p_{total}(\mu) = \frac{k_r}{k_s} p_{ray}(\mu) + \frac{k_m}{k_s} p_{mie}(\mu), \tag{26}$$

$$f_{sca}(\mu) = p_{total}(\mu) \sin(\mu). \tag{27}$$

Finally, G_n is redefined as $G_n(\mu) = \overline{\rho_s} f_{sca}(\mu)/N$.

C. PROPOSED CHANNEL MODEL CONSIDERING THE EFFECTS OF SCATTERING

Based on the mathematical expression of the typical Lambertian channel model, we present the channel model produced by scattering on the optical path T_i-S_n-R_j, which corresponds to the light beam that travels from T_i, interacts with the local scatterrer S_n and reaches R_j. In this context, the DC gain mathematical expression of the scattering optical wireless channel can be written as

$$H_{sca}(0;T_i,S_n,R_j) = \lim_{N\to\infty} \sum_{n=1}^{N} \frac{A_p(m+1)G_n(\mu)}{2\pi D_{i-n-j}^2} \times \cos^m(\phi_{i-S_n}) \cos(\theta_{S_n-j}) rect\left(\frac{\theta_{S_n-j}}{\Theta}\right), \tag{28}$$

where the path length D_{i-n-j} represents the total distance that light travels from the T_i via S_n to the R_j and can be expressed as $D_{i-n-j} = d_{i-S_n} + r_n$. Furthermore, based on the geometry of the Figure 6, the expression d_{i-S_n} can be determined by using the law of cosines as follows:

$$d_{i-S_n} = \sqrt{r_n^2 + d_{ij}^2 - 2 r_n d_{ij} \cos(\beta_{i-S_n})}, \tag{29}$$

where β_{i-S_n} denotes the difference between the angles θ_{i-S_n} and θ_{ij}^{tilt}. The value of β_{i-S_n} depends on the value of these angles and the position of the S_n in the following form:

$$\beta_{i-S_n} = \begin{cases} \theta_{S_n-j} - \theta_{ij}^{tilt} & \text{if } \theta_{ij}^{tilt} < \theta_{S_n-j} \\ \theta_{ij}^{tilt} - \theta_{S_n-j} & \text{otherwise} \end{cases}. \tag{30}$$

To conclude, we now present the general expression of the proposed underground mining VLC channel DC gain as follows:

$$H_{miner}(0;T_i,R_j) = H_{LoS_{(sh)}}(0;T_i,R_j) + H^{(1)}_{NLoS_{(sh)}}(0;T_i,R_j) + H_{sca}(0;T_i,S_n,R_j). \tag{31}$$

The general expression of the underground mining VLC channel model is formed by the addition of expressions (20), (21), and (28). Therefore, we fulfill the objective of including in a single expression all the intrinsic factors of the underground mining scenarios.

VII. RESULTS AND ANALYSIS

In this section, we simulate the CIR, RMS delay spread, and received power based on the proposed underground mining VLC channel model. For the simulation, we choose a tunnel section of dimensions 6m × 3m × 5m. In our analysis, but without losing the generality, we consider a single transmitter and a single receiver, T_1 and R_1, respectively. R_1 is installed on the helmet of mining workers. For a better comparison of the results, an ideal (reference) underground mining scenario and a more realistic (proposed) underground mining scenario are simulated, where the reference VLC channel model and the proposed VLC channel model are included, respectively. These scenarios and their parameters are specified in Table 2. Other system parameters are listed in Table 3.

As the benchmark situation, a reference underground mining scenario is simulated and then compared to the proposed underground mining scenario to discuss and highlight their differences. As mentioned in Section III, the ideal scenario only considers the LoS channel component and the non-LoS components produced by reflections in the walls. Here, two walls are considered to represent the side walls of the tunnel, which are assumed flat and regular. T_1 is installed pointing downwards and R_1 is installed pointing upwards, both located in fixed positions on the tunnel. Finally, in this scenario, neither the shadowing effect nor the scattering effect are considered.

Instead, in the proposed underground mining scenario, we consider five different positions of R_1 in the tunnel. These locations represent the most likely positions that mining workers could have in the tunnel according to their general work area. It should be emphasized that these positions are referential since we assume a single LED and a fixed PD position only to verify the feasibility of the proposed VLC channel model. Generally in underground mines, distributed LED array lighting sources composed of several LEDs are used. In addition, multiple of these LED arrays are distributed throughout the tunnel. Therefore, we would only need superpose all the solutions induced by each LED in order to get the analysis of the total tunnel. Due to the considered characteristics of the proposed underground mining scenario, no matter where R_1 is located, the proposed VLC channel model would work in the same way.

The positions of R_1 are graphically described in Figure 7. For illustrative purposes in all positions, R_1 is tilted and rotated, and its angles of tilt (β_j) and rotation (α_j) are both 45°. Two walls are considered to represent the side walls of the tunnel, which are non-flat and non-regular. This effect is considered in β_w and α_w, which follow a uniform probability distribution, $\beta_w \sim U$[0,180°] and $\alpha_w \sim U$[0,180°]. The effect of shadowing is considered with obstructions entering the tunnel and following the Poisson process described in the Section V, whose intensity parameter ϵ is 5 per minute. Furthermore, for simplicity and model illustration, we consider that the joint probability density functions $f_v(x,y)$ and $g_v(w,h)$ follow a uniform distribution, $f_v(x,y) \sim U$[0,25] and $g_v(w,h) \sim U$[0,2]. The scattering effect is considered by including local scatterers that follow the distribution detailed

This article has been accepted for publication in a future issue of this journal, but has not been fully edited. Content may change prior to final publication. Citation information: DOI 10.1109/ACCESS.2020.3030615, IEEE Access

TABLE 2. Parameters for the underground mining simulation scenarios.

Parameters	Features	
	Reference underground mining scenario	Proposed underground mining scenario
Tunnel:		
Length, X (m)	6	6
Width, Y (m)	3	3
Height, Z (m)	5	5
Wall reflection coefficient, ρ_w	0.6	0.6
Wall rotation angle, α_w (°)	90	U[0,180]
Wall tilt angle, β_w (°)	90	U[0,180]
Scatterer reflection coefficient, ρ_s	0	0.1
Number of scatterers, N	0	40
Transmitter:		
Position, (x,y,z) (m)	(3,0.5,4.5)	(3,0.5,4.5)
Transmitter rotation angle, α_i (°)	0	45
Transmitter tilt angle, β_i (°)	90	45
Receiver:		
Position 1 (x, y, z) (m)	(3,1,1.8)	(3,1,1.8)
Position 2 (x, y, z) (m)	-	(3,1.5,1.8)
Position 3 (x, y, z) (m)	-	(4,2,1.8)
Position 4 (x, y, z) (m)	-	(2.2,2.5,1.8)
Position 5 (x, y, z) (m)	-	(1,2.5,1.6)
Receiver rotation angle, α_j (°)	0	45
Receiver tilt angle, β_j (°)	90	45
Resolution:		
Time resolution (ns)	0.25	0.25
Area elements in X	18	18
Area elements in Y	18	18
Area elements in Z	15	15
Space resolution in X (m)	0.33	0.33
Space resolution in Y (m)	0.16	0.16
Space resolution in Z (m)	0.33	0.33

TABLE 3. System parameters.

Parameters	Values	References
Absolute temperature, T_k (K)	295	[11]
Atmospheric parameter, γ	0.017	[43]
Atmospheric parameter, g	0.72	[43]
Atmospheric parameter, f	0.5	[43]
Average transmitted power, P_i (W)	10	[11]
Background dark current, I_{bg} (nA)	10	[11]
Band-pass filter of transmission	1	[11]
Boltzmann constant, κ (J/K)	1.38×10^{-23}	[11]
Capacitance, C_{pd} (F)	112×10^{-8}	[11]
Disc shaped area radius, R_r (m)	1	[35], [36]
Electronic charge, q (C)	1.6×10^{-19}	[11]
FET channel noise factor, Γ	1.5	[11]
FET trans-conductance, g_m (S)	0.03	[11]
Gain of the optical filter, $g(\cdot)$	1	[11]
Half angle FoV, $\Theta/2$ (°)	70	[13], [30]
Joint probability density, $g_v(w, h)$	U[0,2]	[30]
Joint probability density, $f_v(x, y)$	U[0,25]	[30]
Lambertian mode number, m	1	[35], [36]
Mie scattering coefficient, k_m	U[0,10]	[33], [34]
Noise bandwidth factor, I_2	0.562	[11]
Noise bandwidth factor, I_3	0.0868	[11]
Open-loop voltage gain, G	10	[11]
Physical active area, A_p (cm^2)	1	[11]
Rayleigh scattering coefficient, k_r	U[0.1,0.01]	[33], [34]
Reflective element area, ΔA_w (cm^2)	1	[11]
Refractive index, η	1.5	[11]
Responsivity, R_{PD} (A/W)	0.53	[11]
Semi-angle at half power, $\Phi_{i1/2}$ (°)	60	[11]

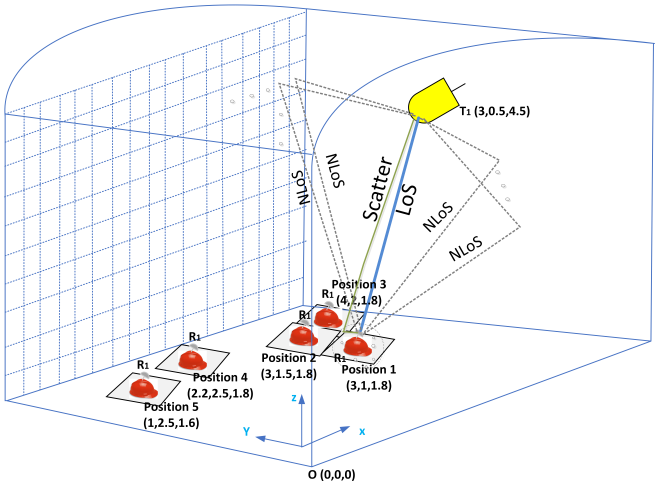

FIGURE 7. Proposed simulation scenario for five different positions of R_1.

in Section VI. The number of local scatterers (N) is set at 40 [35], [36]. The analysis of this value and its variations is carried out in Section VII-A2.

A. ANALYSIS OF THE PROPOSED UNDERGROUND MINING CHANNEL IMPULSE RESPONSE

To evaluate the derived underground mining VLC channel model and confirm the accuracy of our approach, we present the CIRs for the five positions of R_1. These CIRs, each represented by $h_{miner}(t; T_i, R_j)$ are defined as the received optical intensity when the transmitted optical intensity is a unit-area Dirac delta function. Therefore $h_{miner}(t; T_i, R_j)$ can be obtained from expression (31), by adding the delta components $\delta(\cdot)$ that depend on the distance the light beam travels as follows:

$$\begin{aligned} h_{miner}(t; T_i, R_j) &= h_{LoS_{(sh)}}(t; T_i, R_j)\delta\left(t - \frac{d_{ij}}{c}\right) \\ &+ h^{(1)}_{NLoS_{(sh)}}(t; T_i, R_j)\sum_{w=1}^{W}\delta\left(t - \frac{d_{iw} + d_{wj}}{c}\right) \\ &+ h_{sca}(t; T_i, S_n, R_j)\sum_{n=1}^{N}\delta\left(t - \frac{D_{i-n-j}}{c}\right). \end{aligned} \tag{32}$$

Given a number of rays including LoS, non-LoS, and scattering, we compute the detected power and path lengths from T_1 to R_1 for each ray. Then, these data are processed to produce the CIRs. To compare the results of the CIR, we find it convenient to assume that the transmitted power is 1 W.

Figure 8 shows the CIRs for the five positions of R_1 in the proposed underground mining scenario. The number of partitions is set to 18 for X and Y, and 15 for Z. The spacial resolution is set to 0.33 m for X and Z, and 0.16 m for Y. The temporal resolution is set to 0.25 ns (see Table 2). The distance represented in the Figure 8 is the referential Euclidean distance between T_1 and R_1. We observed in all R_1 positions that the LoS component has a higher contribution in

This article has been accepted for publication in a future issue of this journal, but has not been fully edited. Content may change prior to final publication. Citation information: DOI 10.1109/ACCESS.2020.3030615, IEEE Access

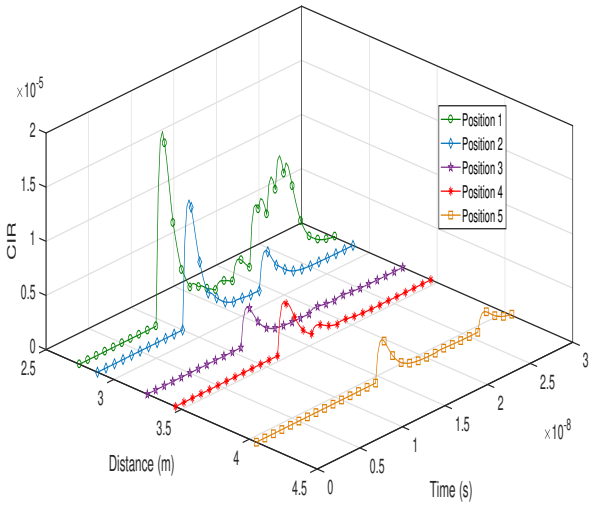

FIGURE 8. CIRs of the five R_1 positions in the evaluated underground mining scenario.

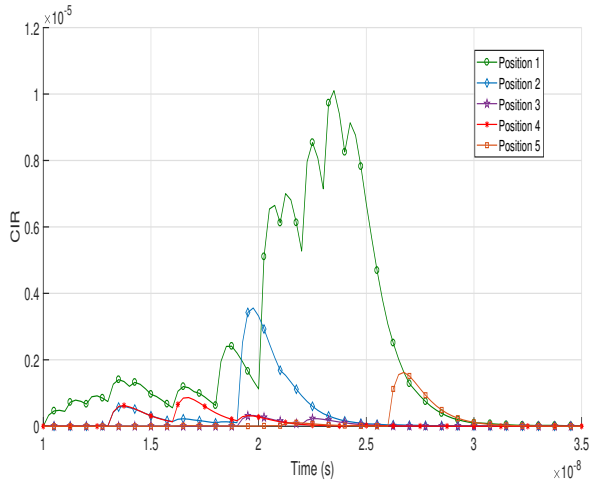

FIGURE 9. CIRs considering the sum of the non-LoS components of the five positions of R_1 in the evaluated underground mining scenario.

the CIR compared to the non-LoS and scattering components. However, the non-LoS and scattering components tend to add a significant amount of power to the total CIR. Furthermore, these components arrive later than the LoS component.

If we compare the CIRs in the Figure 8, several interesting findings can be distinguished. Firstly, as the distance between T_1 and R_1 increases, the underground mining CIR decreases and its propagation delay increases, as well as the rising edge of the CIR becomes less abrupt. However, we note that although the distance from position 3 of R_1 is less than the distance from positions 4 and 5, the CIR of position 3 is the smallest. This behavior occurs because the effect of shadowing is greater in that scenario due to the position of R_1. In this position, the optical link is more likely to be partially or totally blocked due to the physical characteristics of the obstructions entering the tunnel. Secondly, the results show that the obstructions affect all underground mining scenarios. However, the position least affected by shadowing is the position 1 due to the proximity of R_1 to T_1. It is important to mention that both the LoS component and the non-LoS components are affected by shadowing.

1) CHANNEL IMPULSE RESPONSE PRODUCED BY NON-LOS COMPONENTS

To develop an in-depth analysis of each channel component that contributes to the underground mining CIR, Figure 9 shows the CIRs of the sum of all the non-LoS components of the five positions of R_1. These CIRs in all the scenarios maintain the trend of the total CIRs, that is, the greater the distance between T_1 and R_1, the smaller the magnitude of the CIR and the longer the propagation time. We also note that due to bouncing on the walls, the non-LoS component travels a greater distance since leaving T_1 compared to the distance the LoS component travels. Therefore, the non-LoS components arrive at R_1 with a longer delay than the LoS component. The effect of non-flat walls by having uniform random α_w and β_w in a specific interval causes non-LoS components of various magnitudes without marking an increasing or decreasing trend with respect to time. On the other hand, we note that shadowing directly affects non-LoS components depending on the location of R_1. This factor makes the position 1 the least affected and the position 3 the most affect, even though the latter has a shorter distance between T_1 and R_1 compared to positions 4 and 5.

2) CHANNEL IMPULSE RESPONSE PRODUCED BY SCATTERING COMPONENTS

To analyze the channel components produced by scattering, Figure 10 illustrates the CIRs produced by scattering in the five positions of R_1 for the proposed underground mining scenario. It is possible to notice that although each position increases the distance between T_1 and R_1, the magnitude of the CIR is not drastically decreased among R_1 positions. In fact, it is observed that the maximum magnitudes of the CIRs of position 1 and 2 are approximately equal, as well as the maximum magnitudes of positions 3, 4 and 5, with slight differences. This effect is because each local scatter follows the UDSM distribution. Therefore, since the position of the local scatter with respect to R_1 is random, the distance between the local scatter and T_1 will also be variable, so the CIR will not depend solely on the distance between T_1 and R_1. Furthermore, we consider a gain (G_n) that depends on a general phase function gain that randomly combines Rayleigh and Mie scattering, which directly influences similar magnitudes between scenarios.

On the other hand, we note that when the distance between T_1 and R_1 increases, the scattering components reach R_1 later, maintaining the same trend as the LoS and non-LoS components. However, if we compare the arrival times per position of the non-LoS CIRs (Figure 9) with the arrival times per position of the scattering CIRs (Figure 10), we observe that for scattering they are lower. This is due to two factors: 1)

This article has been accepted for publication in a future issue of this journal, but has not been fully edited. Content may change prior to final publication. Citation information: DOI 10.1109/ACCESS.2020.3030615, IEEE Access

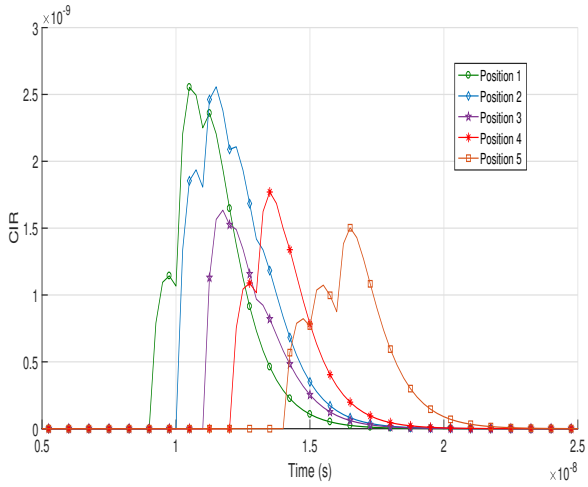

FIGURE 10. CIRs of the scattering components for the five positions of R_1 in the evaluated underground mining scenario.

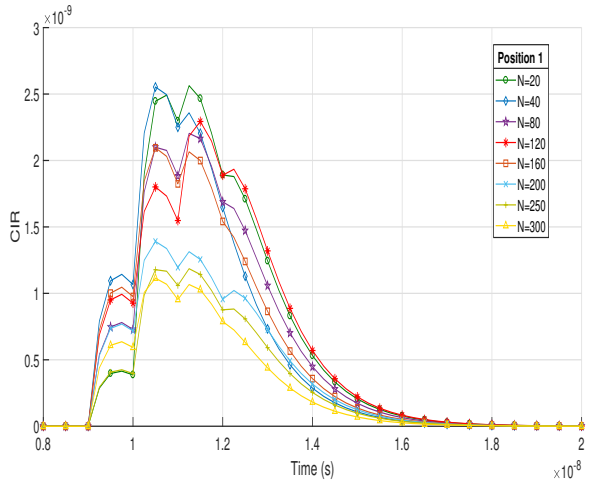

FIGURE 11. CIRs of the scattering component with different values of N for the position 1 of R_1 in the evaluated underground mining scenario.

We only consider the optical path that starts from T_1, bounces off the local scatterer and reaches R_1. Therefore, the distance that the optical signal travels is less compared to the distance of the optical path starting from T_1 going to the wall and reaching R_1. 2) Since the local scatters are much closer to R_1 (disk-shaped area), the signal bounce in the local scatter would reach R_1 faster if we compare it with the proximity of the wall with R_1. Finally, we can deduce that due to the size of the local scatterers (dust particles) the magnitude of the scatterer CIRs in all the positions is smaller compared to the CIRs non-LoS and LoS. However, this magnitude is not negligible and contributes with a factor of the total mining CIR.

For illustrative purposes, and to analyze the effect of the variation and amount of local scatterers, we only choose position 1 of R_1 and vary its values of N as can seen in Figure 11. We can notice that with values of N=20 and N=40, the maximum magnitude of the CIR remains approximately the same. Furthermore, with these values of N, the CIR reaches the maximum values in comparison with the other values of N. As the value of N decreases, the magnitude of the CIR also decrease. This is because the gain factor (G_n) in the CIR is inversely proportional to N. Although we theoretically assume that $N \to \infty$ (see expression (28)), not all optical signal bounces in local scatterers and reach R_1. This would depend on the optical signal being inside the FoV of R_1. Therefore, with this analysis, we can verify that the value of N (N=40) chosen for all the positions of R_1, allows us to develop a feasible simulation model with reasonable complexity. Furthermore, and not least, it is correct in terms of generating a greater contribution from the CIR of the scatterer, which is superimposed to the total underground mining CIR.

B. COMPARATIVE ANALYSIS BETWEEN THE REFERENCE AND PROPOSED UNDERGROUND MINING CHANNEL IMPULSE RESPONSES

To discuss the differences between the proposed underground mining channel model and the reference underground mining channel model, we chose position 1 of R_1 for illustrative purposes. We present their respective CIRs in Figure 12. As we described at the beginning of this section, the characteristics of the reference underground mining scenario are deterministic. Furthermore, it is considered neither shadowing nor scattering. As we can notice, because the distance between T_1 and R_1 for both scenarios is the same, both CIRs have the same delay. However, the differences in magnitudes and temporal evolution are notable. In the first instance, we observe that the magnitude of the LoS part that makes up the CIR of the reference underground mining scenario is 3.489×10^{-5} while for the proposed underground mining scenario it is 1.772×10^{-5}. This is a magnitude reduction of 50.78%. This decrease occurs because in the proposed scenario, the obstructions that generate shadowing severely affect the LoS link.

On the other hand, we also observe that the non-LoS components of the CIR that belong to the proposed underground mining scenario have a greater contribution compared to the reference underground mining scenario. This effect can be best observed in Figure 13. In the reference underground mining scenario the magnitude of the maximum non-LoS contribution is 4.002×10^{-6} while for the proposed underground mining scenario it is 2.434×10^{-6}. The effect of shadowing also negatively affects the non-LoS components in the proposed underground mining scenario. Compared to the LoS contribution, the magnitude of the maximum non-LoS contribution in the proposed underground mining scenario represents 13.73%. However, for the reference underground mining scenario, the magnitude of the maximum non-LoS contribution represents 11.47% with respect to the LoS contribution. The effect of non-flat walls in the proposed

This article has been accepted for publication in a future issue of this journal, but has not been fully edited. Content may change prior to final publication. Citation information: DOI 10.1109/ACCESS.2020.3030615, IEEE Access

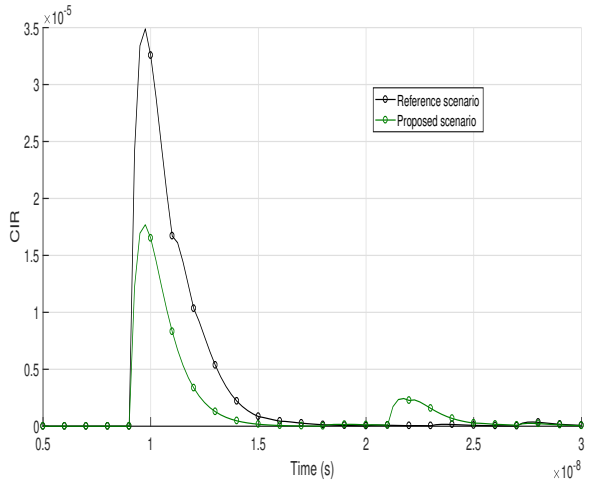

FIGURE 12. Comparison between the total CIR in the reference underground mining scenario and the total CIR in the evaluated underground mining scenario for position 1 of R_1.

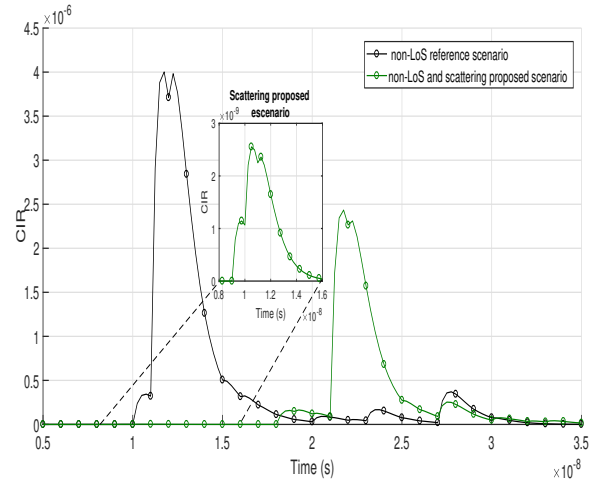

FIGURE 13. Comparison between the CIR of the non-LoS component in the reference underground mining scenario and the CIR of the non-LoS and scattering components in the evaluated underground mining scenario for position 1 of R_1.

underground mining scenario is also highlighted, we can observe greater variability in the magnitudes that make up the CIR.

Finally we see in Figure 13 the contribution of scattering in the proposed underground mining scenario and its time delay. Compared to the LoS contribution, the maximum scattering contribution is approximately 0.75%. However, because it is close in time to the LoS pulse and broad in time terms (almost 1 ns), it modifies and affects the falling edge of the LoS pulse of the total underground mining CIR.

C. TEMPORAL DISPERSION ANALYSIS OF THE PROPOSED UNDERGROUND MINING CHANNEL

In wireless communication systems, due to the own nature of the media and multi-path reflections, the channel stretches the signal transmission in time. This phenomenon is well known as temporal dispersion. Therefore, since we are analyzing a VLC channel characterized by reflections and scattering, we find it more practical and effective to adopt a channel estimator. This estimator must be a parameter that directly reports on the temporal dispersion suffered by the CIR $h_{miner}(t, T_i, R_j)$. A detailed observation of this time parameter provides direct information about the channel configuration. Thus, the initial delay until the first pulse appears is proportional to the length of the LoS path. Any delay measured longer than the initial delay is called an excess delay and corresponds to the existence of pulses after the main pulse, which are non-negligible contributions to the total CIR. Following the above reasoning, the parameter that quantifies the temporal dispersion of the CIR is the RMS delay spread defined as [9], [35]

$$D_{RMS} = \sqrt{\frac{\int_0^\infty (t-\mu_{RMS})^2\, h^2_{miner}(t, T_i, R_j)dt}{\int_0^\infty h^2_{miner}(t, T_i, R_j)dt}}, \quad (33)$$

where the mean delay spread μ_{RMS} is given by [9], [35]

$$\mu_{RMS} = \frac{\int_0^\infty t\, h^2_{miner}(t, T_i, R_j)dt}{\int_0^\infty h^2_{miner}(t, T_i, R_j)dt}. \quad (34)$$

It should be noted that μ_{RMS} strongly depends on the time that the transmitted pulse takes to propagate from T_1 to R_1 after undergoing a reflection, while the D_{RMS} considers only the stretching of the CIR over time. In practice, we consider $h_{miner}(t, T_i, R_j)$ as the sum of samples numeric of all the channel components that form it, so the approximate numeric expressions for D_{RMS} and μ_{RMS} are as follows:

$$D_{RMS} = \sqrt{\frac{\sum_{p=0}^{P} (p\Delta t-\mu_{RMS})^2\, h^2_{miner}(p\Delta t, T_i, R_j)}{\sum_{p=0}^{P} h^2_{miner}(p\Delta t, T_i, R_j)}}, \quad (35)$$

$$\mu_{RMS} = \frac{\sum_{p=0}^{P} p\Delta t\, h^2_{miner}(p\Delta t, T_i, R_j)}{\sum_{p=0}^{P} h^2_{miner}(p\Delta t, T_i, R_j)}, \quad (36)$$

where $p\Delta t$ is discretized quantity of t with a maximum number of samples P. We must emphasize that D_{RMS} is critical in high-speed applications, where the maximum bit rate (R_b) is $R_b \leq 1/10 D_{RMS}$ [9], [35].

We have applied the analysis of this subsection and the expressions (35) and (36) to obtain the characteristic D_{RMS} of $h_{miner}(t, T_i, R_j)$ over the entire proposed underground mining scenario, as depicted in Figure 14. In addition, the main statistical parameters of channel time dispersion are shown in Table 4. These parameters are: mean (μ), standard deviation (σ), 90th percentile $(90\%ile)$, and 100th percentile $(100\%ile)$.

We consider the entire proposed underground mining scenario according to the dimensions and temporal and spatial resolution of Table 2. The maximum and minimum values of the D_{RMS} are 8.28×10^{-9} and 9.01×10^{-12} respectively. Therefore, the maximum R_b that we can reach is 1.20×10^{7} bps. On the other hand, we observe from the Figure 14 that the D_{RMS} distribution is totally non-uniform and with high variability compared to ideal indoor scenarios [9], [44]

This article has been accepted for publication in a future issue of this journal, but has not been fully edited. Content may change prior to final publication. Citation information: DOI 10.1109/ACCESS.2020.3030615, IEEE Access

TABLE 4. Statistics of the temporal parameters of the proposed underground mining channel.

	Statistics			
	$\mu\ (s)$	$\sigma\ (s)$	90%ile (s)	100%ile (s)
D_{RMS}	2.09×10^{-9}	1.77×10^{-9}	4.58×10^{-9}	8.28×10^{-9}
μ_{RMS}	1.74×10^{-8}	4.72×10^{-9}	2.48×10^{-8}	3.59×10^{-8}

or referential underground mining scenarios [13]. This high variability effect is due to non-flat walls and scattering that we consider in the proposed underground mining environment. As these characteristics are modeled with random parameters, the temporal dispersion of the signals does not have a certain trend.

D. ANALYSIS OF THE RECEIVED POWER IN THE EVALUATED UNDERGROUND MINING SCENARIO

An important metric in all communication systems that allows us to verify and analyze the behavior of the channel is the power received at the receiver. For our proposed underground mining scenario, since we consider a single LED along with a single PD, the power received by R_1 due to the light emitted by T_1 is expressed as [9]

$$P_r(R_1) = R_{PD}P_t h_{miner}(0; T_1, R_1) + N_{R1}, \tag{37}$$

where $P_r(R_1)$ is the power received of R_1, R_{PD} is the PD responsivity, and P_t is the emitted optical power by T_1. N_{R1} is the additive noise in R_1 that includes two types of noise that particularly affect underground mining environments, shot noise and thermal noise whose variances are denoted as σ^2_{shot} and $\sigma^2_{thermal}$ respectively. These variances are determined by the following expressions [9], [45]:

$$\sigma^2_{shot} = 2qR_{PD}P_r B_n + 2qI_{bg}I_2 B_n, \tag{38}$$

$$\sigma^2_{thermal} = \frac{8\pi\kappa T_k}{G}\eta A_p I_2 B_n^2 + \frac{16\pi^2\kappa T_k \Gamma}{g_m} C_{pd}^2 A_p^2 I_3 B_n^3. \tag{39}$$

σ^2_{shot} contains two components. The former corresponds to photon fluctuation noise or quantum noise, where q is the electric charge constant and B_n is the bandwidth of the electrical filter that follows the PD. The latter corresponds to the dark current and excess noise, where I_{bg} is the background current due to the ambient light and the noise bandwidth factor is I_2. In $\sigma^2_{thermal}$, the former and latter components represent the feedback-resistor noise and field-effect transistor (FET) channel noise, respectively. Here, κ is Boltzmann's constant, T_k is absolute temperature, G is the open-loop voltage gain, C_{pd} is the fixed capacitance of PD per unit area, Γ is the FET channel noise factor, g_m is the FET trans-conductance, and I_3 is the noise bandwidth factor [9], [45]. The values of these components are defined in Table 3.

Figure 15 shows the cumulative distribution function (CDF) of the power received by R_1 throughout the proposed underground mining scenario. In addition, we insert the graphical distribution of the power received in the evaluated underground mining scenario. We evaluate the power

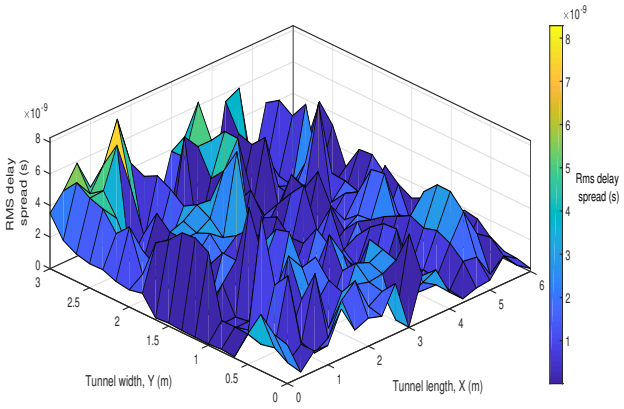

FIGURE 14. RMS delay spread distribution of the proposed underground mining channel model within the evaluated underground mining scenario.

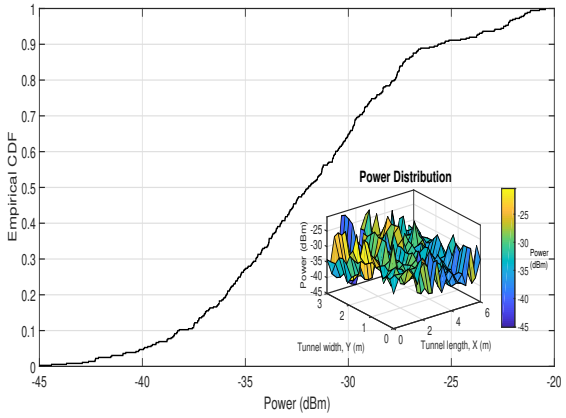

FIGURE 15. Empirical CDF and distribution of the received power in the plane of R_1 for the evaluated underground mining scenario.

received by maintaining the z-coordinate of R_1 with a value of 1.8 m because it is a typical height value for a miner with a helmet. Furthermore, P_t is fixed at 10 W, to also provide consistent lighting in the tunnel. The maximum and minimum values of the received power are -20.43 dB and -45.10 dB, respectively. From the received power CDF we obtain its μ, σ, and $90\%ile$, whose values are -31.87 dB, 4.91 dB, and -25.58 dB, respectively. If we compare these values with VLC indoors scenarios or referential underground mining scenarios, it can be seen that the received power in the proposed underground mining scenario is the least [9], [13]. Furthermore, the received power distribution in the proposed scenario is not always directly proportional to the distance between T_1 and R_1. Therefore, we note that the effect of the rotation and tilt of T_1 and R_1, non-flat walls, and shadowing are influential on the received optical power levels. In order to mitigate the effects of the proposed channel model, and therefore the received power, it is necessary to apply proper channel estimation and equalization schemes, optical modulation systems, and channel coding techniques.

The proposed underground mining VLC channel model

considers the most important characteristics of an underground mining scenario. Therefore, the proposed model will be a great contribution to the future design of systems or applications based on VLC in these type of harsh environments. However, future work is required to fully validate experimentally the proposed model. Among the future work to be done, we consider the most crucial tasks as follows: (1) Experimental validation of the proposed channel model in a real underground mining scenario. (2) Obtaining experimental statistics of the position, rotation and tilt of the optical receiver and develop empirical models. (3) Obtaining experimental statistics of the rotation and tilt of the non-flat walls of the underground mining tunnel and develop empirical models.

VIII. CONCLUSION

In this paper, we proposed a novel VLC channel model for underground mines. The derived model is different to the traditional indoor VLC channel model due to the special characteristics found in underground mining environments. In particular, five main factors make the underground mine channel model unique and different. These unique features are the following: randomly rotated and tilted optical transmitters, randomly rotated and tilted optical receivers, non-flat tunnel walls, presence of obstructions that randomly enter the underground mining scenario that could cause shadowing, and the presence of dust particles that could originate scattering. In order to reasonably present the proposed underground mining VLC channel model, we derived the mathematical analytical expressions of the overall DC channel gain, the underground mining VLC CIR, the RMS delay spread, and the received power in the receiver plane. With these expressions, we verified the validity of the proposed model through numerical experiments within a representative section of a tunnel. Furthermore, we simulated a reference underground mining VLC channel in a referential underground mining scenario, which was compared to the proposed underground mining VLC channel. The simulated data was obtained using a ray tracing methodology. The obtained results demonstrate the notable differences between the proposed underground mining VLC channel model and the reference VLC channel model. In the proposed channel model, the power of the LoS component is reduced by 50.78% compared to the reference channel model. This is mainly due to shadowing, as well as the position and orientation of the transmitter and receiver. Regarding the total magnitude of the proposed underground mining CIR, the non-LoS components have a greater contribution compared to the non-LoS contributions in the reference CIR. This is due to the effect of the non-flat walls, which generate variability in the magnitudes of the non-LoS components. Finally, we have the presence of scattering components that generate temporal dispersion in the proposed total underground mining CIR. The distribution of the RMS delay spread in the entire underground mining environment and its main statistics were found. The impact of non-flat walls and scattering is evidenced by the high variability of the temporal dispersion. Finally, the CDF of the received power and its total distribution in the underground mining scenario were revealed. An in-depth discussion of these parameters demonstrated that the effects of non-flat walls and shadowing are evident in the magnitude of the received power and its variability across the underground mining scenario.

REFERENCES

[1] M. T. Diogo, "European legal framework related to underground mining and tunnelling concerning commission directive (eu) 2017/164, 31 january establishing a fourth list of indicative occupational exposure limit values," International Journal of Mining Science and Technology, 2020.

[2] A. Ranjan, Y. Zhao, H. B. Sahu, and P. Misra, "Opportunities and challenges in health sensing for extreme industrial environment: Perspectives from underground mines," IEEE Access, vol. 7, pp. 139 181–139 195, 2019.

[3] T. Novak, D. P. Snyder, and J. L. Kohler, "Postaccident mine communications and tracking systems," IEEE Transactions on Industry Applications, vol. 46, no. 2, pp. 712–719, 2010.

[4] S. Yarkan, S. Guzelgoz, H. Arslan, and R. R. Murphy, "Underground mine communications: A survey," IEEE Communications Surveys Tutorials, vol. 11, no. 3, pp. 125–142, 2009.

[5] A. F. G. Gonçalves Ferreira, D. M. A. Fernandes, A. P. Catarino, and J. L. Monteiro, "Localization and positioning systems for emergency responders: A survey," IEEE Communications Surveys Tutorials, vol. 19, no. 4, pp. 2836–2870, 2017.

[6] P. Palacios Játiva, C. A. Azurdia-Meza, M. Román Cañizares, D. Zabala-Blanco, and C. Saavedra, "Propagation features of visible light communication in underground mining environments," in Applied Technologies. Springer International Publishing, 2020, pp. 82–93.

[7] U. I. Minhas, I. H. Naqvi, S. Qaisar, K. Ali, S. Shahid, and M. A. Aslam, "A WSN for monitoring and event reporting in underground mine environments," IEEE Systems Journal, vol. 12, no. 1, pp. 485–496, mar 2018.

[8] P. H. Pathak, X. Feng, P. Hu, and P. Mohapatra, "Visible light communication, networking, and sensing: A survey, potential and challenges," IEEE Communications Surveys & Tutorials, vol. 17, no. 4, pp. 2047–2077, 2015.

[9] Z. Ghassemlooy, Optical wireless communications: System and channel modelling with MATLAB. Boca Raton, FL: CRC Press, 2018.

[10] P. P. Játiva, C. A. Azurdia-Meza, M. R. Cañizares, S. Céspedes, and S. Montejo-Sánchez, "Performance enhancement of vlc-based systems using diversity combining schemes in the receiver," in 2019 IEEE Latin-American Conference on Communications (LATINCOM), 2019, pp. 1–6.

[11] P. Palacios Játiva, M. Román Cañizares, C. A. Azurdia-Meza, D. Zabala-Blanco, A. Dehghan Firoozabadi, F. Seguel, S. Montejo-Sánchez, and I. Soto, "Interference mitigation for visible light communications in underground mines using angle diversity receivers," Sensors, vol. 20, no. 2, p. 367, 2020.

[12] F. Miramirkhani and M. Uysal, "Channel modeling and characterization for visible light communications," IEEE Photonics Journal, vol. 7, no. 6, pp. 1–16, 2015.

[13] J. Wang, A. Al-Kinani, W. Zhang, C. Wang, and L. Zhou, "A general channel model for visible light communications in underground mines," China Communications, vol. 15, no. 9, pp. 95–105, 2018.

[14] A. Al-Kinani, C. Wang, L. Zhou, and W. Zhang, "Optical wireless communication channel measurements and models," IEEE Communications Surveys Tutorials, vol. 20, no. 3, pp. 1939–1962, 2018.

[15] G. Wu and J. Zhang, "Demonstration of a visible light communication system for underground mining applications," DEStech Transactions on Engineering and Technology Research, no. iect, 2016.

[16] F. Seguel, "Robust localization system using visible light communication technology for underground mines," Theses, Université de Lorraine ; Universidad de Santiago de Chile, Mar. 2020. [Online]. Available: https://hal.univ-lorraine.fr/tel-02863495

[17] D. Iturralde, C. Azurdia-Meza, N. Krommenacker, I. Soto, Z. Ghassemlooy, and N. Becerra, "A new location system for an underground mining environment using visible light communications," in 2014 9th International Symposium on Communication Systems, Networks Digital Sign (CSNDSP), 2014, pp. 1165–1169.

[18] D. Iturralde, F. Seguel, I. Soto, C. Azurdia, and S. Khan, "A new vlc system for localization in underground mining tunnels," IEEE Latin America Transactions, vol. 15, no. 4, pp. 581–587, 2017.

[19] A. Dehghan Firoozabadi, C. Azurdia-Meza, I. Soto, F. Seguel, N. Krommenacker, D. Iturralde, P. Charpentier, and D. Zabala-Blanco, "A novel frequency domain visible light communication (vlc) three-dimensional trilateration system for localization in underground mining," Applied Sciences, vol. 9, no. 7, p. 1488, 2019.

[20] I. Soto, R. Nilson Rodrigues, G. Massuyama, F. Seguel, P. Palacios Játiva, C. A. Azurdia-Meza, and N. Krommenacker, "A hybrid vlc-rf portable phasor measurement unit for deep tunnels," Sensors, vol. 20, no. 3, p. 790, 2020.

[21] J. Wang, A. Al-Kinani, J. Sun, W. Zhang, and C. Wang, "A path loss channel model for visible light communications in underground mines," in 2017 IEEE/CIC International Conference on Communications in China (ICCC), 2017, pp. 1–5.

[22] J. Wang, A. Al-Kinani, W. Zhang, and C. Wang, "A new vlc channel model for underground mining environments," in 2017 13th International Wireless Communications and Mobile Computing Conference (IWCMC), 2017, pp. 2134–2139.

[23] M. M. Céspedes and A. García Armada, "Characterization of the visible light communications during the construction of tunnels," in 2019 16th International Symposium on Wireless Communication Systems (ISWCS), 2019, pp. 356–360.

[24] Y. Zhai and S. Zhang, "Visible light communication channel models and simulation of coal workface energy coupling," Mathematical Problems in Engineering, vol. 2015, 2015.

[25] S. Riurean, O. Stoicuta, M. Leba, A. Ionica, and Á. Rocha, "Underground channel model for visible light wireless communication based on neural networks," in World Conference on Information Systems and Technologies. Springer, 2020, pp. 293–305.

[26] T. Komine and M. Nakagawa, "A study of shadowing on indoor visible-light wireless communication utilizing plural white led lightings," in 1st International Symposium onWireless Communication Systems, 2004., 2004, pp. 36–40.

[27] Y. Xiang, M. Zhang, M. Kavehrad, M. S. Chowdhury, M. Liu, J. Wu, and X. Tang, "Human shadowing effect on indoor visible light communications channel characteristics," Optical Engineering, vol. 53, no. 8, p. 086113, 2014.

[28] H. Farahneh, C. Mekhiel, A. Khalifeh, W. Farjow, and X. Fernando, "Shadowing effects on visible light communication channels," in 2016 IEEE Canadian Conference on Electrical and Computer Engineering (CCECE), 2016, pp. 1–5.

[29] Y. Wang, X. Wu, and H. Haas, "Load balancing game with shadowing effect for indoor hybrid lifi/rf networks," IEEE Transactions on Wireless Communications, vol. 16, no. 4, pp. 2366–2378, 2017.

[30] Z. Dong, T. Shang, Y. Gao, and Q. Li, "Study on vlc channel modeling under random shadowing," IEEE Photonics Journal, vol. 9, no. 6, pp. 1–16, 2017.

[31] A. Borhani and M. Pätzold, "Time-of-arrival, angle-of-arrival, and angle-of-departure statistics of a novel simplistic disk channel model," in 2011 5th International Conference on Signal Processing and Communication Systems (ICSPCS), 2011, pp. 1–7.

[32] A. Borhani and M. Patzold, "A unified disk scattering model and its angle-of-departure and time-of-arrival statistics," IEEE Transactions on Vehicular Technology, vol. 62, no. 2, pp. 473–485, 2013.

[33] Y. Sun, C. Gong, Z. Xu, and Y. Zhan, "Link gain and pulse width broadening evaluation of non-line-of-sight optical wireless scattering communication over broad spectra," IEEE Photonics Journal, vol. 9, no. 3, pp. 1–12, 2017.

[34] W. Liu, D. Zou, and Z. Xu, "Modeling of optical wireless scattering communication channels over broad spectra," JOSA A, vol. 32, no. 3, pp. 486–490, 2015.

[35] A. Al-Kinani, C. Wang, H. Haas, and Y. Yang, "Characterization and modeling of visible light communication channels," in 2016 IEEE 83rd Vehicular Technology Conference (VTC Spring), 2016, pp. 1–5.

[36] ——, "A geometry-based multiple bounce model for visible light communication channels," in 2016 International Wireless Communications and Mobile Computing Conference (IWCMC), 2016, pp. 31–37.

[37] S. Shen, S. Li, and H. Steendam, "Simultaneous position and orientation estimation for visible light systems with multiple leds and multiple pds," IEEE Journal on Selected Areas in Communications, pp. 1–1, 2020.

[38] D. Plets, S. Bastiaens, L. Martens, and W. Joseph, "An analysis of the impact of led tilt on visible light positioning accuracy," Electronics, vol. 8, no. 4, p. 389, 2019.

[39] D. Kim, J. K. Park, and J. T. Kim, "Three-dimensional vlc positioning system model and method considering receiver tilt," IEEE Access, vol. 7, pp. 132 205–132 216, 2019.

[40] M. A. Arfaoui, M. D. Soltani, I. Tavakkolnia, A. Ghrayeb, C. Assi, M. Safari, and H. Haas, "Measurements-based channel models for indoor lifi systems," arXiv preprint arXiv:2001.09596, 2020.

[41] Y. S. Eroğlu, Y. Yapıcı, and Güvenç, "Impact of random receiver orientation on visible light communications channel," IEEE Transactions on Communications, vol. 67, no. 2, pp. 1313–1325, 2019.

[42] M. D. Soltani, A. A. Purwita, Z. Zeng, H. Haas, and M. Safari, "Modeling the random orientation of mobile devices: Measurement, analysis and lifi use case," IEEE Transactions on Communications, vol. 67, no. 3, pp. 2157–2172, 2019.

[43] H. Ding, "Modeling and characterization of ultraviolet scattering communication channels," Ph.D. dissertation, UC Riverside, 2011.

[44] S. S. Muhammad, "Delay profiles for indoor diffused visible light communication," in 2015 13th International Conference on Telecommunications (ConTEL), 2015, pp. 1–5.

[45] J. Kahn and J. Barry, "Wireless infrared communications," Proceedings of the IEEE, vol. 85, no. 2, pp. 265–298, 1997.